iScience

CellPress
OPEN ACCESS

Article

NLRC5 affects diet-induced adiposity in female mice and co-regulates peroxisome proliferator-activated receptor PPARγ target genes

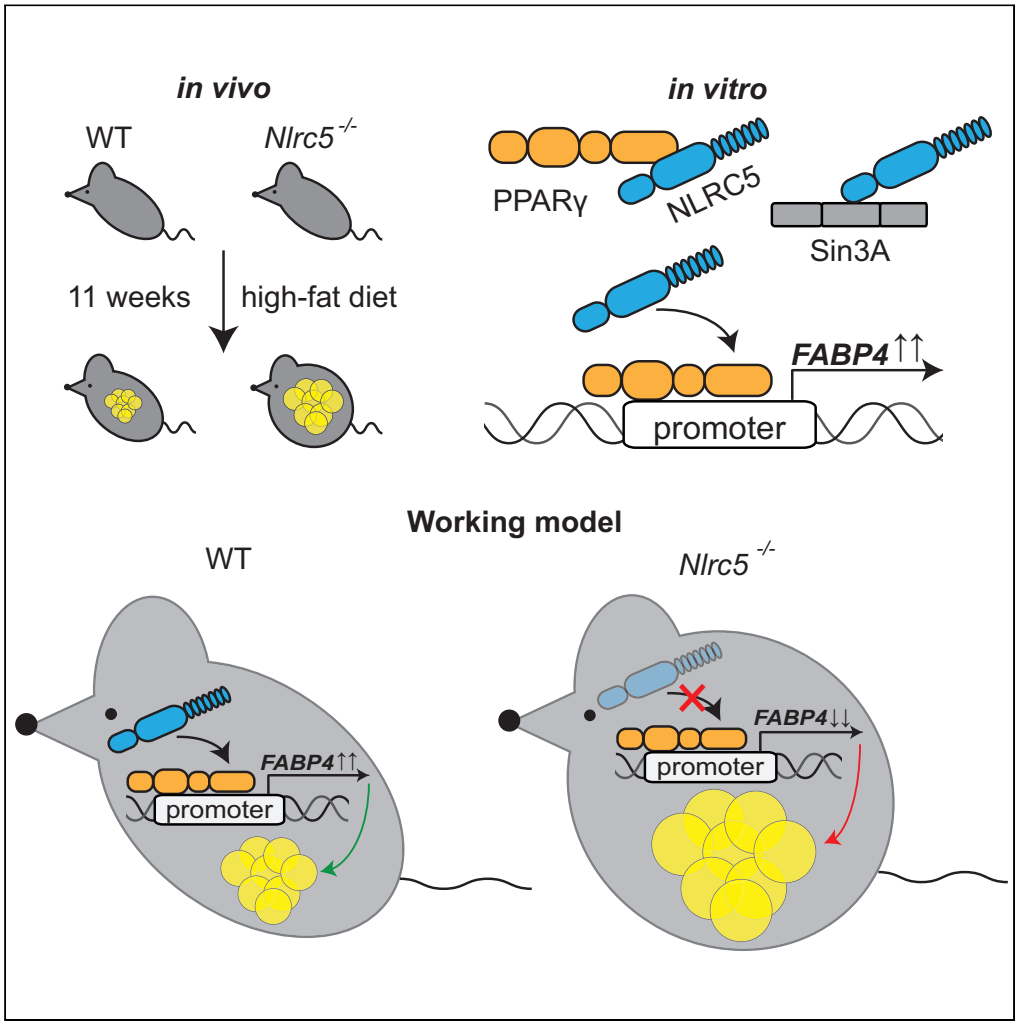

Sarah Bauer, Vanessa Aeissen, Alena M. Bubeck, ..., Philip Rosenstiel, W. Florian Fricke, Thomas A. Kufer

thomas.kufer@uni-hohenheim.de

Highlights

Female *Nlrc5*$^{-/-}$ mice on HFD gain more weight compared to WT animals

NLRC5 interacts with PPARγ and synergistically co-regulates PPARγ target genes

NLRC5 interacts with Sin3A and NELFB

Sin3A fine-tunes NLRC5-mediated transcription of PPARγ targets

Bauer et al., iScience 26, 106313
April 21, 2023
https://doi.org/10.1016/j.isci.2023.106313

iScience

CellPress
OPEN ACCESS

Article

NLRC5 affects diet-induced adiposity in female mice and co-regulates peroxisome proliferator-activated receptor PPARγ target genes

Sarah Bauer,[1] Vanessa Aeissen,[1] Alena M. Bubeck,[2] Ioannis Kienes,[1] Kornelia Ellwanger,[1,5] Mona Scheurenbrand,[2] Fjolla Rexhepi,[3] Sheela Ramanathan,[3] Philip Rosenstiel,[4] W. Florian Fricke,[2] and Thomas A. Kufer[1,6,*]

SUMMARY

Nucleotide-binding and oligomerization domain containing 5 (NLRC5) is the key transcriptional regulator of major histocompatibility (MHC) class I genes. Recent observations suggest a role for NLRC5 in metabolic traits and in transcriptional regulation beyond MHC class I genes. To understand the function of NLRC5 in metabolic disease, we subjected *Nlrc5*$^{-/-}$ mice to high-fat diet (HFD) feeding. Female *Nlrc5*$^{-/-}$ mice presented with higher weight gain and more adipose tissue (AT) compared to wild-type (WT) animals. Mechanistically, we demonstrate that NLRC5 enhanced the expression of peroxisome proliferator-activated receptor (PPAR) γ target genes in human cells. We identify Sin3A and negative elongation factor (NELF) B as two novel NLRC5 interaction partners and show that Sin3A partly modulates the synergistic transcriptional effect of NLRC5 on PPARγ. Collectively, we show that NLRC5 contributes to weight gain in mice, which involves transcriptional enhancement of PPARγ targets by NLRC5 that is co-regulated by Sin3A.

INTRODUCTION

The rates of obesity have increased alarmingly fast in the last decades, especially in countries with a Western industrialized lifestyle.[1] According to data from the World Health Organization (WHO), the prevalence of obesity worldwide has nearly tripled from 1975 to 2016, with 13% of the world's adult population being obese in 2016. The excess of adipose tissue (AT), which is the main characteristic of obesity, is accompanied by several comorbidities, including the metabolic syndrome (MetS).[2] Since the discovery that the AT produces tumor necrosis factor α (TNF-α) in a mouse model of high-fat diet (HFD)-induced obesity,[3] it has become more and more evident that our immune system plays an important role in the development and maintenance of obesity-associated comorbidities (reviewed in[4]). One of the most obvious examples for the close interconnection of obesity and immunological responses is the chronic state of low-grade, sterile inflammation, which is a pathological feature of the MetS, as well as type 2 diabetes mellitus (T2DM) and other obesity-associated comorbidities. This low-grade inflammatory response is believed to originate mainly from the AT, with AT-resident macrophages (ATM) playing a key role in the development of the inflammatory status associated with obesity.[5–7] The key mediators of the innate immune system are pattern-recognition receptors (PRR) which recognize microbe-associated molecular patterns (MAMPs) or danger-associated molecular patterns (DAMPs) and in the following induce a pro-inflammatory response.[8,9] It was shown that knockout (KO) or knockdown of PRRs improved obesity-associated comorbidities and inflammation in mice and human and murine cells.[10,11] Nucleotide-binding and oligomerization domain (NOD)-like receptors (NLRs) are a group of cytosolic PRRs all sharing a common tripartite structure, consisting of a central NACHT (oligomerization module, present in NAIP, CIITA, HET-E, TP-1) domain, a variable number of C-terminal leucine-rich repeats (LRRs) and a varying N-terminal effector domain.[12] The major function of NLR proteins is to protect the host from invading pathogens by triggering innate immune responses.[13] However, in the last years increasing evidence has been presented that NLRs are also involved in the low-grade inflammatory status associated with obesity and obesity-associated comorbidities (reviewed in[14]). Genetic deficiency of the NLR protein NOD1 in mice reduced HFD-induced AT inflammation, weight gain and insulin resistance (IR).[15–17] In humans, NOD1 expression is increased in

[1]Department of Immunology, Institute of Nutritional Medicine, University of Hohenheim, 70599 Stuttgart, Germany

[2]Department of Microbiome and Applied Bioinformatics, Institute of Nutritional Science, University of Hohenheim, 70599 Stuttgart, Germany

[3]Department of Immunology and Cell Biology, Faculty of Medicine and Health Sciences, Université de Sherbrooke, Sherbrooke, Québec J1H 5N4, Canada

[4]Institute of Clinical Molecular Biology, Christian-Albrechts University of Kiel, 24105 Kiel, Germany

[5]Present address: Institute of Medical Genetics and Applied Genomics, University Hospital Tübingen, Calwerstrasse 7, 72076 Tübingen, Germany

[6]Lead contact

*Correspondence: thomas.kufer@uni-hohenheim.de

https://doi.org/10.1016/j.isci.2023.106313

patients with T2DM,[18] gestational diabetes[19] and MetS.[20] For the NLR protein NLRP3, similar effects have been reported, with *Nlrp3* KO in mice leading to reduced IR, AT-infiltration of macrophages and insulin and glucose levels in the serum and protection against HFD-induced, interleukin (IL) -1β-mediated β-cell fibrosis.[21–23] In humans, NLRP3 and IL-1β levels in the AT are positively correlated with the extent of obesity and IR.[24–27] In contrast with NOD1 and NLRP3, the NLR proteins NOD2 and NLRP12 have been shown to confer protective roles in obesity and associated morbidities in mice.[28–31]

Unlike most NLR proteins, the NLR protein Nucleotide-binding and oligomerization domain containing 5 (NLRC5) does not function as a classical PRR and its activating ligand here thereto is unknown. Instead, NLRC5 has been described as the transcriptional master regulator of the major histocompatibility complex (MHC) class I genes by several groups.[32–36] To mediate this transcriptional regulation, NLRC5 is shuttling into the nucleus and is, because of lacking a DNA binding domain (DBD), binding to promoters of MHC class I genes indirectly via the so-called MHC enhanceosome.[37–39] Beside its main function as a transcriptional regulator, roles of NLRC5 in NF-kB[40–46] and interferon (IFN) regulation,[34,41,45,47,48] malignant transformation[49–53] and inflammasome activation[46,54,55] have been described, suggesting multiple biological activities of NLRC5. Recently, NLRC5 has also been implicated in metabolic traits. *NLRC5* was identified as a candidate gene to affect high-density lipoprotein cholesterol (HDL-C) levels in humans[56] and single nucleotide polymorphisms (SNP) in *NLRC5* and its promotors have been associated with altered triglyceride levels as well as dyslipidaemia.[57,58] Moreover, specific DNA methylation patterns of the *NLRC5* locus are associated with obesity and body mass index (BMI) in a Ghanaian cohort.[59] In mice, a contribution of Nlrc5 to HFD-induced diabetic nephropathy[60] and myocardial damage[61] was reported. Together, these studies strongly support novel roles of NLRC5 in metabolism and body weight regulation. However, the underlying mechanisms remain elusive.

The peroxisome proliferator-activated receptor (PPAR) γ is a nuclear receptor belonging to the steroid receptor superfamily and functions as a ligand-activated transcription factor.[62] PPARγ is expressed in brown AT, large intestine and spleen, but the highest levels are found in white AT.[63] In line with its expression pattern, PPARγ is considered the master regulator of adipogenesis.[64–67] Heterozygous expression of a dominant negative version of PPARγ as well as AT-specific *Pparg* KO in mice results in the development of lipodystrophy and IR.[68,69] Accordingly, the dominant negative mutation PPARγ Pro495Leu is resulting in reduced AT generation and the development of IR causing T2DM and hypertension.[70,71] The PPARγ gene contains separate promotors, which together with alternative splicing gives rise to two different PPARγ isoforms, PPARγ1, and PPARγ2, a longer version with additional 28 amino acids at the N-terminus in humans.[63,72,73] Activation of PPARγ in adipocytes leads to the expression of proteins involved in lipid metabolism and accumulation and drives adipocyte differentiation.[74,75] One important PPARγ target is the fatty acid-binding protein (FABP) 4. FABP4 maintains adipocyte homeostasis and regulates lipolysis and adipogenesis through interaction with the hormone-sensitive lipase (HSL) and PPARγ, respectively.[76,77]

In this study, we show that *Nlrc5* deficiency in female mice leads to higher body weight and larger adipose tissues and adipocyte size on HFD. Furthermore, we confirm the interaction between the NACHT domain of NLRC5 and the master regulator of adipogenesis, PPARγ, and show that NLRC5 in synergy with PPARγ regulates PPARγ target genes that are involved in lipid metabolism. Lastly, we identify two novel NLRC5 interaction partners, Sin3A and NELFB, and unravel a potential role of Sin3A in the syngeristic regulation of PPARγ targets by NLRC5 and PPARγ.

RESULTS

Female *Nlrc5*$^{-/-}$ mice on HFD present with higher body weight gain and an increase in adipose tissue

To investigate the effect of NLRC5 in HFD-induced obesity, 8-week-old female *Nlrc5*$^{-/-}$ mice (Figure S1) and wild-type (WT) littermate controls were fed an HFD, containing 30% crude fat, or a control diet (ctrl.) matched in protein content, containing 4% crude fat, for 11 weeks. As expected, all animals on HFD gained significantly more weight compared to animals on control diet. Of interest, *Nlrc5*$^{-/-}$ mice on HFD gained significantly more weight compared to WT animals on HFD (Figure 1A, Table S2). The higher weight gain of *Nlrc5*$^{-/-}$ animals on HFD was not because of hyperphagia, as *Nlrc5*$^{-/-}$ and WT animals on both diets consumed similar amounts of food (Figure 1B) and metabolizable energy intake was similar between both genotypes on ctrl. or HFD (WT[ctrl.] 0.28 MJ/mouse/week; *Nlrc5*$^{-/-}$[ctrl.] 0.28 MJ/mouse/week; WT

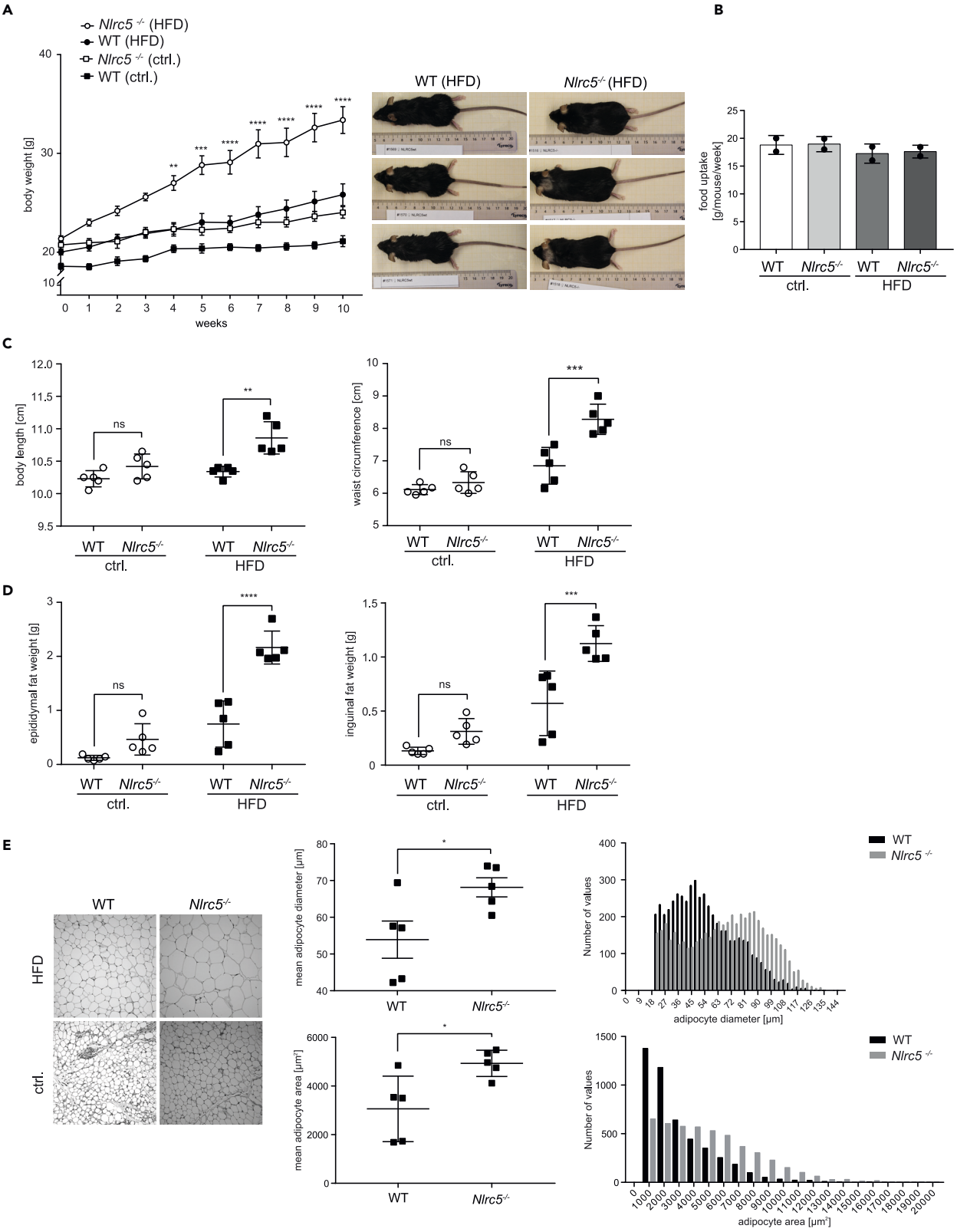
A
Nlrc5 -/- (HFD)
WT (HFD)
Nlrc5 -/- (ctrl.)
WT (ctrl.)
body weight [g]
weeks
WT (HFD)
Nlrc5-/- (HFD)
B
food uptake [g/mouse/week]
WT
Nlrc5-/-
ctrl.
HFD
C
body length [cm]
waist circumference [cm]
ns
D
epididymal fat weight [g]
inguinal fat weight [g]
E
HFD
ctrl.
mean adipocyte diameter [µm]
mean adipocyte area [µm²]
Number of values
adipocyte diameter [µm]
adipocyte area [µm²]

Figure 1. *Nlrc5* deficiency aggravates HFD-induced obesity

Female WT and *Nlrc5*$^{-/-}$ mice (n = 5) were fed a control (ctrl.) or high-fat diet (HFD) for 11 weeks.

(A) Body weight of mice over course of feeding and representative pictures of WT and *Nlrc5*$^{-/-}$ mice after 11 weeks of HFD feeding. Data show mean ± S.D. of 5 animals per condition for each of the indicated time points.

(B) Average food uptake per mouse per week. Data show mean ± S.D. of two cages with two or three animals.

(C) Mouse body lengths and waist circumferences after 11 weeks of feeding. Data show mean ± S.D.

(D) Weights of epididymal and inguinal fat depots after 11 weeks of feeding. Data show mean ± S.D.

(E) Average adipocyte diameter and area in PFA fixed epididymal adipose tissue sections of WT and *Nlrc5*$^{-/-}$ mice after 11 weeks of HFD feeding. Left: representative pictures of PFA fixed epididymal adipose tissue sections from WT and *Nlrc5*$^{-/-}$ mice on ctrl. or HFD; middle: mean adipocyte diameter or mean adipocyte area per mouse, data show mean ± S.D.; right: histogram showing distribution of adipocytes by diameter or by area, data show pooled results of 5 animals per condition. *p ≤ 0.0332, **p ≤ 0.0021, ***p ≤ 0.0002, and ****p < 0.0001 two-way ANOVA with Tukey's multiple comparisons test (A, C, D; adjusted p value) or unpaired t-test (E). See also Figures S1 and S2 and Table S2.

[HFD] 0.36 MJ/mouse/week; *Nlrc5*$^{-/-}$[HFD] 0.37 MJ/mouse/week). *Nlrc5*$^{-/-}$ mice on HFD presented with significantly increased body length and, in accordance with the higher body weight, with increased waist circumference compared to WT animals (Figure 1C, Table S2). No difference in body length and waist circumference was observed for *Nlrc5*$^{-/-}$ and WT animals on control diet (Figure 1C, Table S2). The higher increase in body weight of the *Nlrc5*$^{-/-}$ animals was, at least in parts, because of an increase in body fat mass. *Nlrc5*$^{-/-}$ animals at the end of the experiment presented with significantly larger epididymal and inguinal AT depots compared to WT animals. Of interest, this effect was already evident, albeit not statistical significant, for the KO animals on control diet, and largely reinforced by HFD feeding (Figure 1D, Table S2). Because of this very pronounced effect of *Nlrc5* KO on AT, we took a closer look into fixed epididymal AT sections of *Nlrc5*$^{-/-}$ and control animals on HFD. *Nlrc5*$^{-/-}$ mice presented with larger adipocytes (Figure 1E, left panel) with increased mean adipocyte diameter and mean adipocyte area (Figure 1E, middle panel). In accordance, the size distribution of adipocytes in the epididymal AT shifted toward larger adipocytes in the *Nlrc5*$^{-/-}$ compared to the WT animals (Figure 1E, right panel). Of interest, in contrast to the highly increased weight gain and AT formation, *Nlrc5*$^{-/-}$ mice on HFD presented with a trend to reduced serum cholesterol (Figure S2A) and reduced serum triglyceride levels (Figure S2B) compared to WT controls. A trend to reduced triglyceride levels was also observed for *Nlrc5*$^{-/-}$ animals on control diet (Figure S2B). By contrast, mRNA levels of the pro-fibrogenic and pro-inflammatory cytokines Tgf-β and Tnf-α in epididymal AT (Figures S2C and S2D) and liver (Figures S2E and S2F), did not differ significantly between *Nlrc5*$^{-/-}$ and WT animals on both diets. Similar results were obtained in a second independent experiment using 3 mice per group (data not shown).

Thus, *Nlrc5* deficiency in female mice on HFD led to an obesity-like phenotype with increased weight gain and waist circumference, more AT and larger adipocytes in the epididymal AT. However, despite the pronounced adiposity phenotype, lipid metabolism was not impaired nor were inflammatory reactions affected by *Nlrc5* deficiency.

Microbiome composition in *Nlrc5*$^{-/-}$ animals

Certain NLRs, such as NLRP12, may modulate the organismal threshold to obesity by affecting gut microbial community composition.[31] As the effect of NLRC5 on microbiota composition here thereto has not been reported and to investigate if the observed HFD-induced phenotype in our *Nlrc5*$^{-/-}$ animals could be related to microbial alterations in the gut, taxonomic profiling of fecal samples of *Nlrc5*$^{-/-}$ and WT animals via 16S rRNA gene amplicon sequencing was performed. Overall, *Nlrc5*$^{-/-}$ mice showed a reduced microbiota alpha diversity compared to WT mice, which was significant for the HFD group (HFD[KO vs WT]: q = 0.018, control diet[KO vs WT]: q = 0.36, Shannon Index, WRST, Figure S3A). The alpha diversity was also influenced by batch effects (separate amplification runs: p = 0.00025, WRST, Figure S3B), but an even distribution of samples across these two batches, as well as the inclusion of the batch as a fixed effect in subsequent statistical analyses, were used to control for plate effects on compositional microbial analyses. The differences in microbial diversity were accompanied by some alterations of the taxonomic composition as determined by generalized linear mixed models (GLMM). In total, ten bacterial taxa were differentially associated with either diet or genotype alone or the interaction between diet and genotype (Figure 2A).

Altered relative abundances because of *Nlrc5* KO or the HFD only were identified for two genera each. Comparing *Nlrc5* WT to KO mice revealed increased *Ruminococcaceae* UCG 004 (q = 0.015) and decreased *Lachnospiraceae* GCA 900066575 (q = 0.012) relative abundance, whereas in response to the HFD, the genera *Lactobacillus* (q = 0.053) and *Oscillibacter* (q = 0.025) were both increased (GLMM^{FDR},

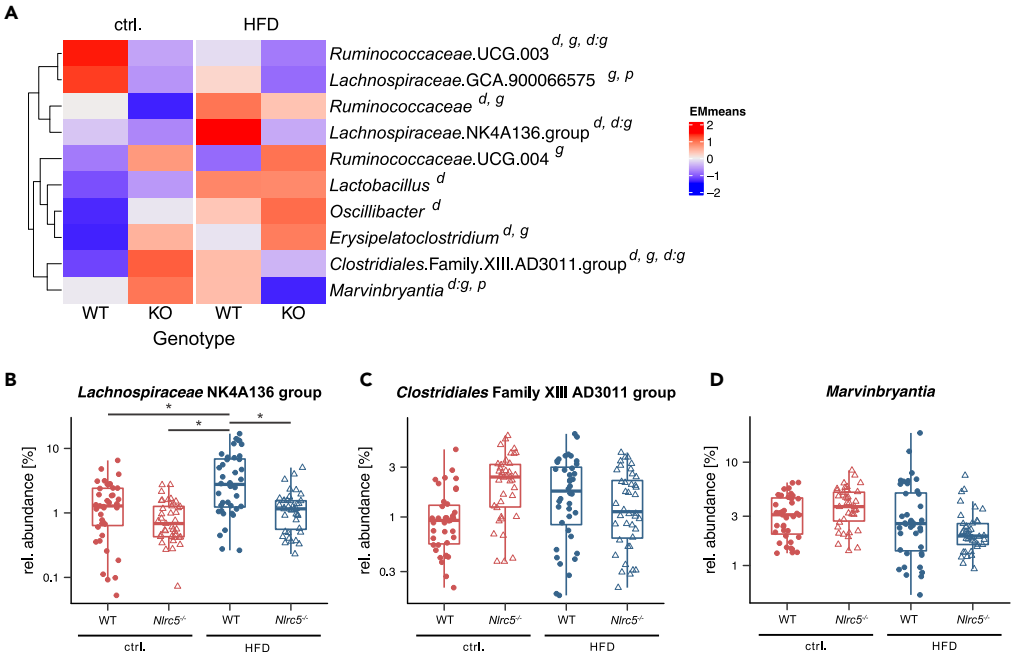

Figure 2. The high-fat diet induced phenotype in *Nlrc5* deficient mice might be associated with the microbiota composition

(A) GLMM analysis modeled with repeated measurements per mouse and littermates as random effects. Significant ($q < 0.05$) associations between relative abundance alterations of microbial groups and dietary intervention (d), gene knock out (g), both (d:g) and technical procedures (p) are shown.

(B–D) Comparisons of estimated marginal means (EMM) by Tukey's test revealed the *Lachnospiraceae* genus to be significantly increased by the high-fat diet (HFD) but not *Nlrc5* deficiency. For the genera *Marvinbryantia* and *Clostridiales* Family XIII AD3011 group only trends of altered relative abundances in response to the diet or gene knock out were observed. Data show median with first and third quartiles and upper and lower Whiskers of in total 39 (ctrl. diet) or 40 (HFD) fecal samples collected from each of the 5 animals per condition at 8 different time points. Relative abundances are displayed on a log-scale. GLMM and Tukey's test p values were BH-corrected with $q \geq 0.05$ ns, $q < 0.05$ *, $q < 0.01$ **, $q < 0.001$ ***. See also Figure S3.

Figure 2A). Four taxa were further significantly associated with diet and genotype concurrently. The genus *Erysipelatoclostridium* was increased by HFD ($q = 0.031$) and *Nlrc5* KO ($q = 0.0027$) independently, whereas the abundance of the family *Ruminococcaceae* was reduced by *Nlrc5* deficiency ($q = 0.0012$) and increased by HFD ($q = 0.03$). The two remaining taxa, *Ruminococcaceae* UCG 003 ($q = 0.013$) and *Clostridiales* Family XIII AD3011 group ($q = 0.006$), as well as the genera *Lachnospiraceae* NK4A136 group ($q = 0.006$) and *Marvinbryantia* ($q = 0.015$) were associated with the interaction of diet and genotype by the GLMM (Figure 2A). However, post-hoc analysis of subgroups by Tukey's test revealed statistical significance only for the *Lachnospiraceae* NK4A136 group. For this genus, HFD significantly increased the relative abundance in WT animals ($q = 0.049$), but not HFD-fed *Nlrc5*$^{-/-}$ mice ($q = 0.044$, Figure 2B). Similar trends were observed for the genus *Clostridiales* Family XIII AD3011 group, were *Nlrc5* deficiency ($q = 0.077$) and HFD ($q = 0.144$) were separately correlated with increased relative abundance, whereas a combination of both diminished the effect ($q = 0.339$, Tukey^{FDR}, Figure 2C). For *Marvinbryantia*, HFD alone did not change the relative abundance in WT animals ($q = 0.574$) but reduced it in KO animals ($q = 0.0625$, Tukey^{FDR}, Figure 2D). Although for this taxon associations with batch effects were identified (Figure S3C), because of the even distribution of samples across both batches, no obvious clustering by diet or genotype was determined which could explain the observed interaction effect of diet and genotype. For *Ruminococcaceae* UCG 003, the diet:genotype interaction was primarily driven by genotype, as the taxon was only present in half of the WT animals and further reduced when mice received HFD ($q = 0.044$, Tukey^{FDR}, Figure S3D).

Taken together, HFD and *Nlrc5* deficiency alone as well as the interaction between diet and genotype influenced taxonomic gut microbiota composition. These microbiota alterations might contribute to the metabolic phenotype observed for *Nlrc5*$^{-/-}$ mice.

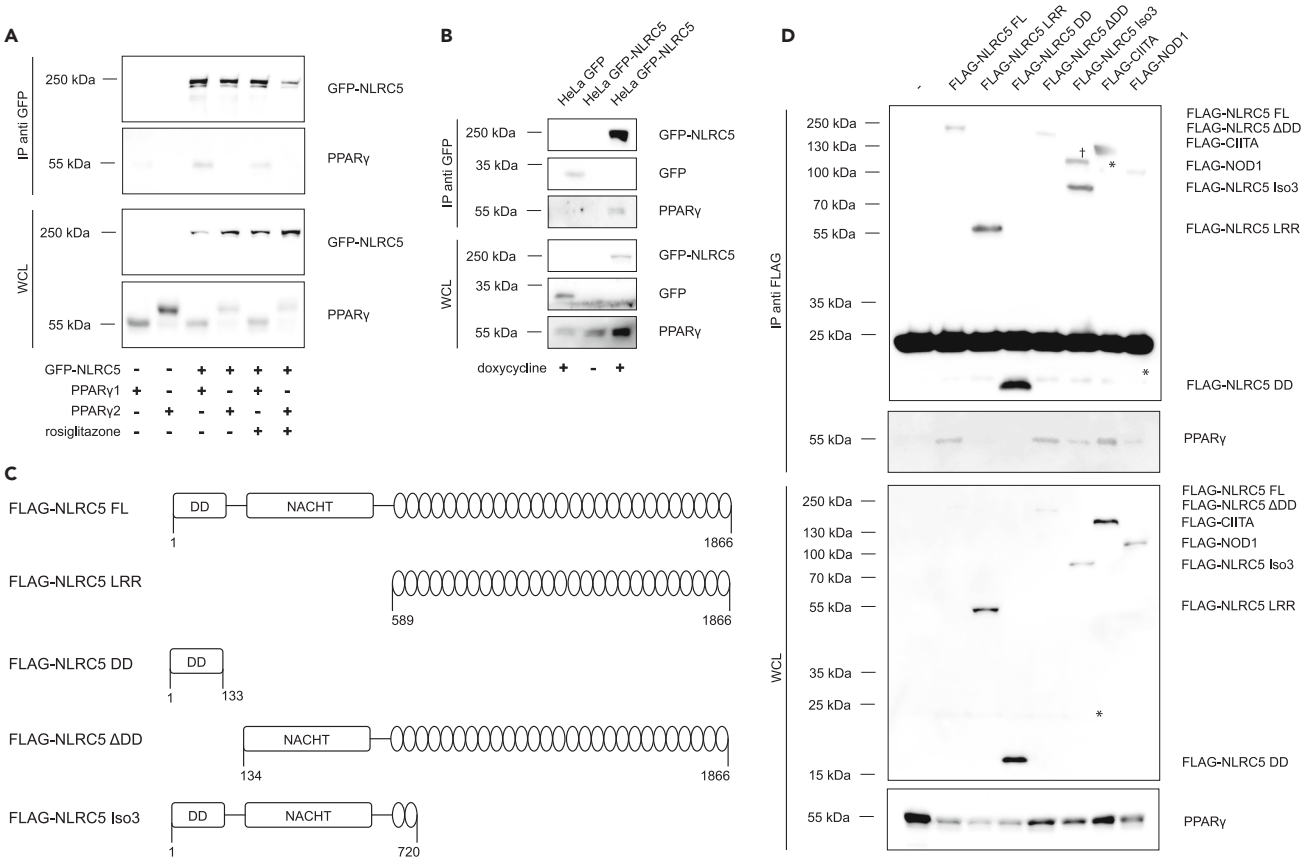

Figure 3. NLRC5 interacts with PPARγ isoform 1 by its NACHT domain

(A) Immunoblots from anti-GFP immunoprecipitations (IP) of HEK293T cells transfected with GFP-NLRC5, PPARγ isoform 1 or PPARγ isoform 2 and stimulated overnight with 0.4 μg/mL rosiglitazone where indicated. IPs and whole cell lysates (WCL) were probed for GFP and PPARγ.

(B) Immunoblots from anti-GFP IPs of HeLa GFP and HeLa GFP-NLRC5 cells induced overnight with 1 μg/mL doxycycline. Blots were probed for GFP and PPARγ.

(C) Domain organization of the NLRC5 constructs used in (D).

(D) Immunoblots from anti-FLAG IPs from HEK293T cells transfected with PPARγ isoform 1 and the indicated FLAG-NLRC5 construct. Blots were probed for FLAG and PPARγ. Representative blots of 1 (B) or 2 (A and D) experiment is shown. †, SDS-stable dimer; *, unspecific bands.

NLRC5 interacts with PPARγ1 via its NACHT domain

PPARγ is the master regulator of adipocyte differentiation.[64–66] As we observed changes in adipocyte size in the *Nlrc5*$^{-/-}$ animals on HFD we wanted to test whether NLRC5 affects PPARγ. To this end, we first tested for protein-protein interactions and used co-expression of either PPARγ isoform 1 or PPARγ isoform 2 with GFP-tagged NLRC5 in HEK293T cells. GFP-NLRC5 specifically co-precipitated with PPARγ1, but not PPARγ2, and activation of PPARγ by treatment with its specific agonist rosiglitazone slightly reduced binding of PPARγ1 to GFP-NLRC5 (Figure 3A). Taking advantage of stable HeLa cell lines with doxycycline-inducible expression of GFP-NLRC5 (HeLa GFP-NLRC5) or GFP (HeLa GFP) as control, the binding of endogenous PPARγ1, but again not PPARγ2, to NLRC5 was confirmed (Figure 3B). This is in line with data showing that NLRC5 interacts with PPARγ in endothelial cell types,[78] albeit the isoform specificity was not addressed by these authors. To map the domain of NLRC5 responsible for interaction, PPARγ1 was expressed together with different FLAG-tagged NLRC5 deletion constructs (Figure 3C) in HEK293T cells and co-immunoprecipitation (co-IP) against FLAG was performed. Co-purification of PPARγ1 was observed for full-length FLAG-NLRC5 (FLAG-NLRC5 FL), for the NLRC5 construct lacking the N-terminal death domain (FLAG-NLRC5 ΔDD) and, to a smaller extent, for NLRC5 isoform 3 (FLAG-NLRC5 Iso3), a naturally occurring NLRC5 isoform lacking most of the LRRs[34] (Figure 3D). Co-immunoprecipitation was neither observed for the N-terminal death domain nor with the C-terminal LRRs (Figure 3D). This binding pattern showed that the NACHT domain of NLRC5 was necessary for interaction with PPARγ1.

As the NACHT domain is a common structural feature of all NLR proteins, FLAG-tagged NOD1 and class II transactivator (CIITA), two other NLR family members that are phylogenetically closely related to NLRC5,[40] were tested for interaction with PPARγ1. CIITA, like NLRC5, functions as transcriptional regulator and is known as the master regulator of MHC class II genes.[79] NOD1 in contrast functions as a classical PRR, recognizing intracellular peptidoglycan and initiating pro-inflammatory responses.[80] PPARγ1 co-immunoprecipitated with FLAG-CIITA to a similar extend as NLRC5 FL. In contrast, no binding over background level of PPARγ1 to FLAG-NOD1 was detected (Figure 3D). Thus, binding of PPARγ1 to the NACHT domain of NLRC5 seems to occur with high specificity, but not exclusivity, as PPARγ1 also co-immunoprecipitated with NLRC5's closest phylogenetic relative, CIITA, but not with NOD1.

In summary, our data showed that PPARγ isoform 1, but not isoform 2, interacts with NLRC5 by its central NACHT domain, proposing a role of NLRC5 in the regulation of PPARγ activity.

NLRC5 enhances transcription of PPARγ target genes

Having demonstrated interaction between NLRC5 and PPARγ1, in a next step we investigated the effects of NLRC5 on PPARγ-mediated transcriptional regulation. To this end, HeLa GFP and HeLa GFP-NLRC5 cells were used which predominantly express PPARγ isoform 1 (Figure S4A). Functionality of the cell lines was verified on protein and mRNA level by immunoblot and qRT-PCR, respectively (Figures 4A and 4B). GFP and GFP-NLRC5 proteins were only detected on doxycycline induction (Figure 4A). As expected, expression of human leukocyte antigen (HLA)-A or-B, two MHC class I molecules, was detectable on protein and mRNA level only in HeLa GFP-NLRC5 cells (Figures 4A and 4B). HLA-A/B was detected in both, induced and uninduced HeLa GFP-NLRC5 cells, to a similar extend (Figures 4A and 4B) because of a very low basal GFP-NLRC5 expression in uninduced cells (Figure 4B). Thus, minor amounts of NLRC5 are sufficient to boost a full MHC class I response, highlighting the potency of NLRC5 as transcriptional regulator. To analyze the influence of NLRC5 on PPARγ transcriptional activity, we measured the expression of cluster of differentiation 36 (CD36) and fatty acid-binding protein 4 (FABP4), two known PPARγ targets. Successful induction of NLRC5 expression was verified on mRNA level (Figure 4C). To activate PPARγ, cells were treated with rosiglitazone. As expected,[81,82] rosiglitazone treatment led to increased expression of both PPARγ targets in HeLa GFP and HeLa GFP-NLRC5 cells (Figure 4C). Expression of NLRC5 by doxycycline treatment alone was sufficient to increase *FABP4* transcription to approximately the levels observed in rosiglitazone stimulated HeLa GFP cells (Figure 4C). As seen for MHC class I genes, even the very low expression of NLRC5 in uninduced HeLa GFP-NLRC5 cells was sufficient to drive *FABP4* transcription (Figure 4C). Simultaneous rosiglitazone treatment and expression of GFP-NLRC5, both, basal and induced, led to a strong synergistic activation of *FABP4* transcription compared to rosiglitazone-treated HeLa GFP cells. As seen for the cells without rosiglitazone treatment, only a slight further increase was observed when inducing the expression of GFP-NLRC5 by doxycycline treatment (Figure 4C). For CD36, similar observations were obtained, although the effect was less pronounced compared to FABP4 (Figure 4C).

To further investigate the positive synergistic effect of NLRC5 on PPARγ-mediated transcription of target genes, the expression of *FABP4* in HeLa GFP and HeLa GFP-NLRC5 cells treated with increasing concentrations of rosiglitazone was analyzed (Figure 4D). As shown above, *FABP4* expression was not detectable in untreated HeLa GFP cells but increased on rosiglitazone treatment, expression peaking at a concentration of 0.2 μg/mL (Figure 4D, white bars). In HeLa GFP-NLRC5 cells, *FABP4* expression was readily detectable without rosiglitazone treatment and treatment of these cells with rosiglitazone potentiated the expression of *FABP4* compared to HeLa GFP cells, validating a synergy in transcriptional activation between NLRC5 and PPARγ. Minor amounts of NLRC5 were sufficient to mediate this synergistic transcriptional activation of *FABP4*, as the leaky expression of NLRC5 in HeLa GFP-NLRC5 cells was sufficient to drive this synergistic effect (Figure 4D, gray bars, middle panel) and induction of NLRC5 expression by doxycycline treatment only slightly further enhanced this effect for the lower concentrations of rosiglitazone (Figure 4D, gray bars, right panel). The synergistic effect of NLRC5 and PPARγ in activating *FABP4* transcription was also verified in HEK293 cell lines expressing GFP or GFP-NLRC5 on doxycycline induction with qualitatively similar results (Figures S4B and S4C). Inhibition of PPARγ by the specific antagonist GW9662 led to complete abrogation of the rosiglitazone-induced increase in *FABP4* transcription in both HeLa GFP and HeLa GFP-NLRC5 cells. GW9662 also abolished the synergistic effect of NLRC5 expression on *FABP4* transcriptional upregulation in HeLa GFP-NLRC5 cells but did not affect NLRC5-induced *FABP4* expression (Figure 4E). These data conclusively support that PPARγ and NLRC5 synergistically drive the transcription of PPARγ target genes.

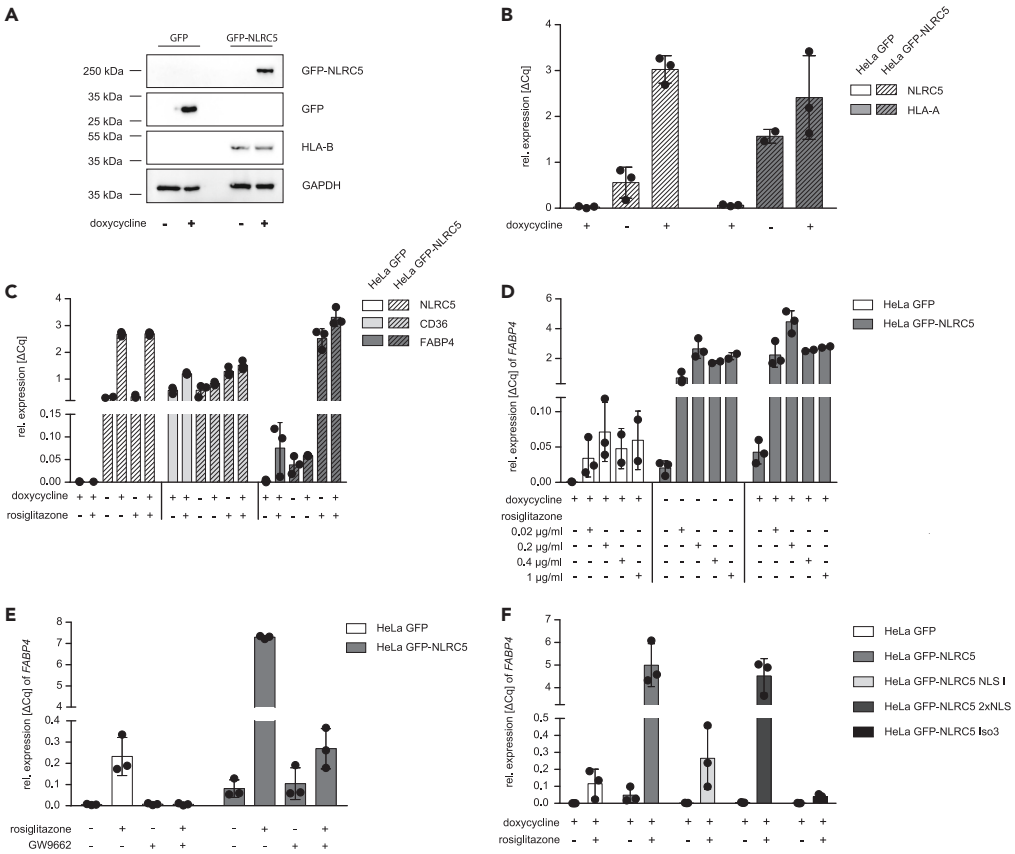

Figure 4. NLRC5 enhances *FABP4* transcription

(A) Immunoblot of protein lysates from HeLa GFP and HeLa GFP-NLRC5 cells, induced overnight with doxycycline where indicated. Probing for GFP, HLA-B and GAPDH as loading control is shown.

(B–F) Expression of *NLRC5* (B and C), *HLA-A* (B), *CD36* (C) and *FABP4* (C–F) in HeLa cell lines expressing GFP, GFP-NLRC5 (B - F) or GFP-tagged NLRC5 mutants (F). (B) HeLa GFP and HeLa GFP-NLRC5 cells were treated with 1 µg/mL doxycycline and 0.1 µg/mL rosiglitazone for 20–24 h, p = 0.0036 (NLRC5)/0.0250 (HLA-A) Kruskal-Wallis test. (C) HeLa GFP and HeLa GFP-NLRC5 cells were treated with 0.2 µg/mL doxycycline and 0.02 µg/mL rosiglitazone 20–24 h, p = 0.0091 (NLRC5)/ 0.0087 (CD36)/0.0091 (FABP4) Kruskal-Wallis test. (D) HeLa GFP and HeLa GFP-NLRC5 cells were treated with 1 µg/mL doxycycline and the indicated concentrations of rosiglitazone for 20–24 h, p = 0.0012 Kruskal-Wallis test. (E) HeLa GFP and HeLa GFP-NLRC5 cells were treated with 1 µg/mL doxycycline, 0.1 µg/mL rosiglitazone and 10 µM GW9662 for 20–24 h, p = 0.0044 Kruskal-Wallis test. (F) HeLa GFP, HeLa GFP-NLRC5 WT or HeLa cells stably expressing GFP-tagged NLRC5 mutants were treated with 1 µg/mL doxycycline and 0.2 µg/mL rosiglitazone for 20–24 h, p = 0.0012 Kruskal-Wallis test. (B–F) Gene expression was determined by qRT-PCR. Data show mean ± S.D. of at least two independent experiments conducted in technical replicates. See also Figures S4 and S5.

PPARγ as a nuclear receptor is localized to the nucleus,[83,84] whereas NLRC5 is predominantly present in the cytoplasm but able to translocate into the nucleus.[32,37,40,85] The nuclear shuttling is mediated by a nuclear localization sequence (NLS) localized between the CARD and NACHT domains of NLRC5.[32] In a next step, we sought to investigate if NLRC5 localization is needed to mediate its synergistic effect with PPARγ on *FABP4* transcription. For this, we used stable HeLa cell lines with doxycycline inducible expression of three different NLRC5 variants which we recently characterized:[37] NLRC5 NLS I harbors a mutation in the NLS rendering it incapable of translocating to the nucleus, NLRC5 2xNLS possesses two SV40 NLS and therefore is predominantly localized to nucleus, and NLRC5 isoform 3, lacking most of the LRR domain, presents with impaired nuclear export and thus is localized predominantly to the nucleus compared to WT NLRC5.[37] Localization of the NLRC5 variants was verified by immunofluorescence (Figure S4D). As seen before, GFP-NLRC5 expression in combination with rosiglitazone treatment led to a strong increase in *FABP4* expression compared to a GFP expressing control cell line (Figure 4F). In contrast, expression of GFP-NLRC5 NLS I did not upregulate *FABP4* and activation of PPARγ in these cells led to a less pronounced increase in *FABP4* transcription compared to HeLa GFP-NLRC5 cells (Figure 4F). As seen in previous work for MHC class I

genes,[37] expression of GFP-NLRC5 Isoform 3 did not induce *FABP4* transcription over the levels in HeLa GFP cells. Expression of GFP-NLRC5 2xNLS failed to induce *FABP4* expression and simultaneous activation of PPARγ in these cells led to a somewhat lower increase in *FABP4* transcription compared to GFP-NLRC5 WT cells (Figure 4F). Thus, nuclear localization, nuclear shuttling, and the NLRC5 C-terminal LRR domain are important for PPARγ target gene activation by NLRC5, confirming a model in which direct interaction in the nucleus is necessary for the observed biological effects.

To substantiate our results obtained in the HeLa cell lines, we used bone marrow-derived macrophages (BMDMs) from WT and *Nlrc5*$^{-/-}$ animals. As NLRC5 has been shown to influence lipopolysaccharide (LPS)-induced pro-inflammatory signaling,[40,41] BMDMs were stimulated with 50 ng LPS for 6 h and Tnf-α secretion was measured by ELISA. To investigate the effect of PPARγ on LPS-induced pro-inflammatory signaling, BMDMs were treated with rosiglitazone overnight before LPS stimulation. LPS stimulation highly induced Tnf-α secretion in both WT and *Nlrc5*$^{-/-}$ cells. *Nlrc5* KO cells showed higher Tnf-α levels compared to WT cells, indicating an anti-inflammatory effect of NLRC5 in the context of LPS-induced pro-inflammatory signaling. In accordance with the literature,[86,87] PPARγ activation by pre-treatment of BMDMs with rosiglitazone markedly reduced Tnf-α secretion. This effect was obvious in both, WT and *Nlrc5* KO cells (Figure S5A). However, in *Nlrc5*$^{-/-}$ BMDMs the reducing effect of rosiglitazone was less stringent as in the WT BMDMs (Figure S5B, 63% reduction of Tnf-α production in WT versus 48% reduction in KO BMDMs). This finding substantiates our results obtained in the HeLa and HEK293T cell lines and points toward a synergistic effect of NLRC5 and PPARγ, not only in PPARγ target gene induction but also in the context of LPS-induced inflammation. This might indicate that besides a direct effect on adipocytes, NLRC5 might also regulate pro-inflammatory macrophages in the AT.

Sin3A and NELFB interact with NLRC5 and Sin3A influences *FABP4* transcription by NLRC5

To identify accessory factors that mediate the effect of NLRC5 on the induction of PPARγ target genes, we screened for novel NLRC5 interaction partners involved in transcriptional regulation. As we recently showed that the N-terminal NLRC5 death domain (DD) has transcriptional activity and confers specificity for MHC class I gene regulation,[33] we performed a yeast two-hybrid (Y2H) screen using the DD of NLRC5 (amino acids 1–139) as bait. Out of 73.5 million interactions tested, 228 clones showed interaction and were sequenced and results ranked according to the predicted biological score (PBS), which takes into account known false positives from other screens.[88] Notably, several importin alpha proteins were identified as interaction partners, providing confidence in the approach, as NLRC5 shuttles into the nucleus in an importin-dependent manner[32] (Table S3). Amongst the very high and high-confidence candidates (PBS scores A and B), Sin3A and negative elongation factor (NELF) B (COBRA1), two known transcriptional regulators, caught our interest. Sin3A is an essential scaffold for the histone deacetylase (HDAC) complex, interacting with eight core proteins, and controls transcription both positively and negatively.[89] NELFB is part of the negative elongation factor (NELF) complex that binds and stalls the RNA polymerase II complex at the promoter region downstream of the transcriptional start site.[90,91] Overlapping the 38 different clones encoding Sin3A fragments identified the interaction site of NLRC5 DD within aa 595–717 of Sin3A, corresponding to the HDAC interaction domain (HID) (Figure 5A, schematic representation). For NELFB three clones were obtained that overlapped in a fragment of aa 57–405 of NELFB (Figure 5B, schematic representation). To validate the data from the Y2H screen, we transiently overexpressed different NLRC5 deletion constructs in HEK293T cells and performed co-IP experiments. These confirmed the binding of NLRC5 FL, NLRC5 Isoform 3 an NLRC5 DD, but not of an NLRC5 construct lacking the DD (ΔDD), to FLAG-Sin3A (Figure 5A). Similar results were obtained from co-IP experiments with NLRC5 deletion constructs and ectopically expressed NELFB, with NELFB co-purifying with NLRC5 FL, Isoform 3 and DD, but not with NLRC5 ΔDD (Figure 5B). These results proof the NLRC5 DD to be both necessary and sufficient for Sin3A and NELFB binding.

As both Sin3A and NELFB function as transcriptional regulators,[89–91] in a next step, we investigated the influence of Sin3A and NELFB on the NLRC5-mediated PPARγ target gene expression. To this end, siRNA-mediated knockdown (KD) of either Sin3A or NELFB was performed in HeLa GFP and HeLa GFP-NLRC5 cells. PPARγ was activated by rosiglitazone treatment after KD and FABP4 mRNA levels were determined by qPCR. As we showed above that the leaky expression of NLRC5 in combination with PPARγ activation was sufficient to induce high levels of *FABP4* transcription, GFP-NLRC5 expression was not actively induced by doxycycline treatment. KD of Sin3A and NELFB led to a significant reduction of the corresponding mRNA level by more than 50% compared to non-targeting control siRNA (siNT) (Figure 5C). As shown

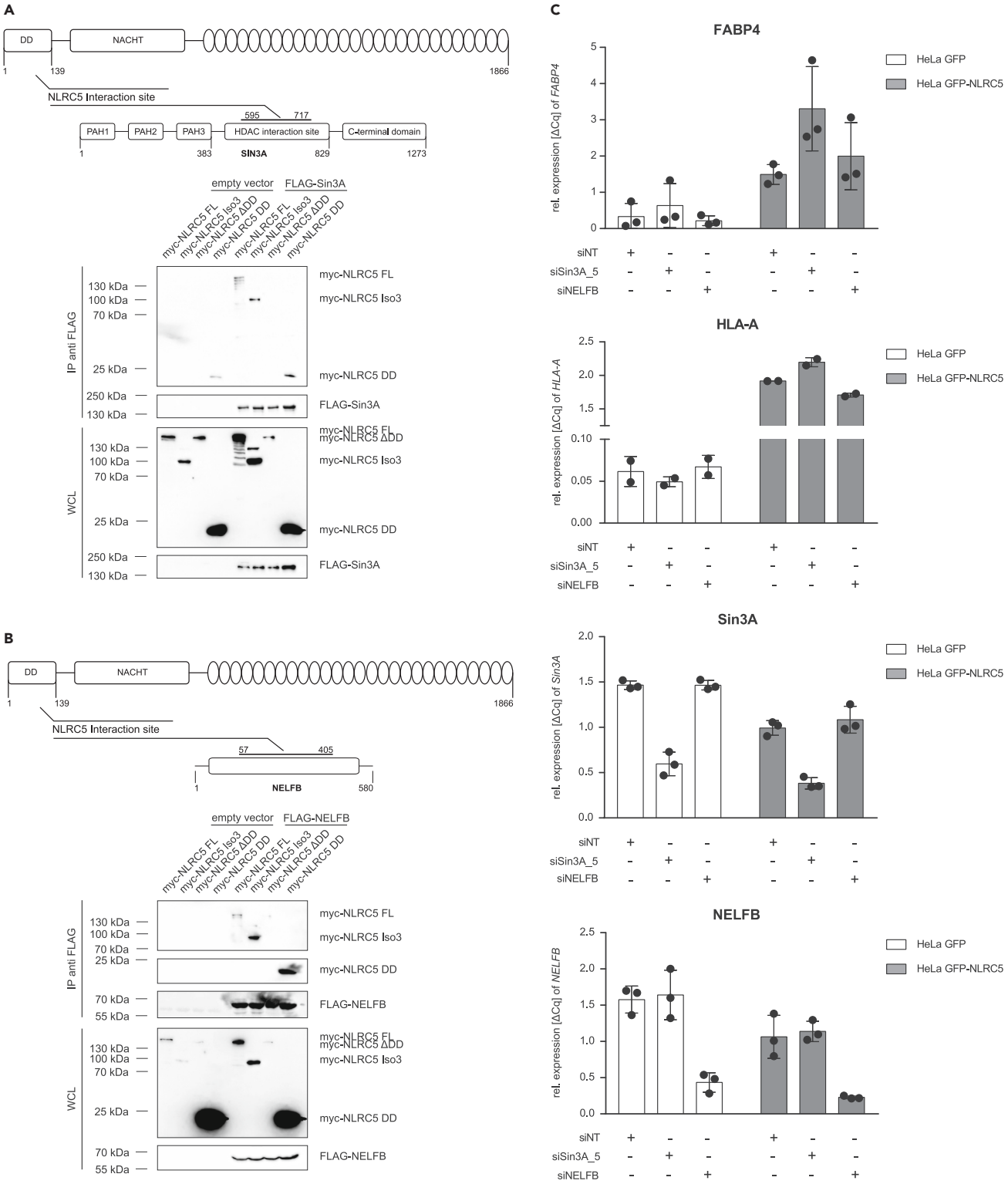

Figure 5. Sin3A interacts with NLRC5 by its death domain and influences *FABP4* induction by NLRC5

(A and B) Upper panel: schematic illustration of NLRC5 interaction with Sin3A (A) and NELFB (B). Lower panel: Immunoblots from anti-FLAG IPs of HEK293T cells expressing the indicated myc-tagged NLRC5 constructs and FLAG-Sin3A (A) or FLAG-NELFB (B), respectively. Blots were probed for myc and FLAG. Representative blot from 3 independent experiments is shown.

Figure 5. *Continued*

(C) *FABP4*, *HLA-A*, *Sin3A* and *NELFB* expression in HeLa GFP and HeLa GFP-NLRC5 cells after siRNA-mediated *Sin3A* or *NELFB* knockdown. Cells were treated with 0.2 μg/mL rosiglitazone for 22 h after 48 h of knockdown. p = 0.0163 (FABP4)/0.0032 (HLA-A)/0.0079 (Sin3A)/0.0110 (NELFB) Kruskal-Wallis test. Gene expression was determined by qRT-PCR. Data show mean ± S.D. of two (HLA-A) or three (FABP4, Sin3A, NELFB) independent experiments. See also Figures S6 and S7.

above, PPARγ activation highly increased transcription of *FABP4* in HeLa GFP-NLRC5 cells compared to HeLa GFP cells. Although KD of NELFB did not affect FABP4 mRNA expression in both cell lines, reduced levels of Sin3A led to an increased expression of *FABP4* in HeLa GFP as well as HeLa GFP-NLRC5 cells compared to cells treated with a non-targeting control siRNA (siNT). Thereby, the effect was more pronounced in HeLa GFP-NLRC5 than in HeLa GFP cells, as Sin3A KD in GFP-NLRC5 expressing cells led to more than a 120% increase in *FABP4* expression compared to a 92% increase in FABP4 mRNA for HeLa GFP cells (Figure 5C). This effect of Sin3A KD was rather specific for the PPARγ target FABP4 as Sin3A KD did not significantly increase HLA-A mRNA levels compared to siNT control (Figure 5C). This was also validated by western blot, where no effect of Sin3A KD on NLRC5-mediated MHC class I protein expression was observed (Figure S6A) and by overexpression of Sin3A, that did not significantly affect NLRC5-mediated B250 promotor activity measured by luciferase reporter assay (Figure S6B).

Taken together, Sin3A and NELFB were identified as novel NLRC5 interacting proteins that associate with NLRC5 via its DD. Of these two known transcriptional regulators, Sin3A contributes to the synergistic transcriptional regulation of FABP4 by NLRC5 and PPARγ.

DISCUSSION

NLRC5 has been identified by us and others as the master regulator of MHC class I genes.[32,33,37] Although MHC class I regulation is undoubtedly a key function, NLRC5, like several other NLR proteins, in the recent years has also been implicated in metabolic traits (reviewed in[14]). Two independent epigenome-wide association studies identified the NLRC5 locus to be differentially methylated in normal weight versus obese individuals, but with conflicting results, with Meeks et al.[59] positively and Cao-Lei et al.[92] negatively associating methylation of the NLRC5 locus with obesity,[59,92] BMI and waist circumference.[59] In most cases, DNA methylation mediates gene repression.[93] Thus, our results are in line with the work of Meeks et al. finding associations of lower accesibility of the NLRC5 locus with obesity.[59] Of interest, another study also reported a trend toward increased weight gain in *Nlrc5* deficient animals on HFD, however without mechanistically elaborating on this finding.[61] *Nlrc5* deficient animals on HFD presented with significantly increased body length compared to HFD-fed WT animals (Figure 1C) which might confound the significantly increased body weight gain for *Nlrc5*$^{-/-}$ animals on HFD. However, when normalizing final body weight to body length, the difference between the two genotypes was still significant (WT (HFD) 2.609 g/cm, S.E.M. 0.147; *Nlrc5*$^{-/-}$ (HFD) 3.272 g/cm, S.E.M. 0.095; adjusted p value 0.0007 two-way ANOVA with Tukey's multiple comparisons test). In this work, we identify a strong adiposity phenotype for female *Nlrc5* deficient mice. We did also include male mice in our feeding study, but the results were inconclusive compared to the strong phenotype in female mice. Further work is needed to adress the potential sex-specificity of *Nlrc5* deficiency in the obesity context.

SNPs in *NLRC5* have been associated with alterations in lipid metabolism.[56–58] Charlesworth et al. showed that SNPs in *NLRC5* significatly correlated with HDL-C levels.[56] In line, Hosseinzadeh et al. correlated SNPs in *NLRC5* with HDL-C, cholesterol and triglyceride levels[57] and one SNP in *NLRC5* (rs2178950) has been associated with low-densitiy lipoprotein (LDL) and total cholesterol dyslipidemia.[58] Together with our observations on reduced serum triglyceride levels for *Nlrc5* KO compared to WT mice (Figure S2B), these data point toward an influence of NLRC5 on lipid metabolism, the nature of which remains to be determined in more detail in further studies.

DNA methylation of *NLRC5* also has been positively associated with circulating TNF-α concentration and inversely correlated with the risk of coronary heart disease.[94] The role of NLRC5 in inflammation is controversially discussed. NLRC5 has been shown to inhibit NF-kB signaling *in vitro* in a HEK293T cell-based reporter gene assay[40,41] and in RAW264.7 macrophages.[43] *In vivo*, Tong et al. found enhanced IL-6 and IFN-β production in *Nlrc5* deficient murine embryonic fibroblasts (MEF), peritoneal macrophages and BMDMs in LPS or vesicular stomatitis virus-challenged *Nlrc5* KO animals.[45] In accordance, accelerated cardiac fibrosis with increased NF-kB activation and Tnf-α and Tgf-β production in *Nlrc5* KO mice on HFD was

reported.[61] In contrast, *Nlrc5* deficiency reduced diabetic kidney injury by supression of NF-kB and reduction of the TGF-β/Smad pathway compared to *Nlrc5* sufficient mice.[60] For some *Nlrc5* KO mouse models, no differences in NF-kB activation and downstream signaling were found.[42,44,46] Our results on increased Tnf-α secretion of *Nlrc5* KO BMDMs is in accordance with the *in vitro*[40,41,43] and some of the *in vivo* data.[45,61] However, in contrast to Ma and Xi,[61] we found no differences in Tnf-α and Tgf-β mRNA levels in liver and epididymal AT of *Nlrc5*$^{-/-}$ and WT animals (Figure S2). This discrepancy might be explained as we examined different tissues (liver and AT vs. heart) and by differences in the study design, as we used females and 11 weeks of intervention compared to male animals and 15 weeks of HFD.[61]

For other NLRs, effects on gut microbiota composition have been reported, that in the case of NLRP12 were associated with weight gain.[31] Fecal microbiome composition analysis by 16S rRNA sequencing revealed 10 bacterial taxa to be significantly altered and seven of those being associated with our dietary intervention. Of those, most (*Ruminococcaceae, Oscillibacter, Lactobacillus, Erysipelatoclostridium* and *Clostridiales* Family XIII*)* have been described to be altered in abundance by HFD or in the obesity context before,[95–98] reflecting our result. Only for *Lachnospiraceae* NK4A136, our data is contradicting the finding of reduced relative abundance upon HFD feeding, as described by others.[99,100] The reasons for this conflicting finding remain to be determined. Of interest, two of the three bacterial groups that were differentially affected by diet:genotype interactions in a broader sense are associated with metabolic traits. *Lachnospiraceae* NK4A136 has been shown to be increased in abundance in rats with T2DM.[101] And the relative abundance of *Marvinbryantia* was increased in rats upon high fructose intake[102] and in rabbits after HFD feeding.[103] The identified alterations in relative abundance were only small and based on compositional data, which does not allow conclusion to be drawn about absolute changes of specific bacteria.[104] Still, these microbial changes could partially contribute to the phenotype of *Nlrc5* KO animals. This should be subject of further studies.

NLRC5 functions as a transcriptional regulator of MHC class I and associated genes.[32,39,105,106] As NLRC5 is devoid of a *bona fide* DNA binding domain (DBD), its association with chromatin is mediated indirectly via the MHC enhanceosome complex,[37] a multiprotein DNA binding complex binding to conserved S/X/Y motifs in MHC class I gene promotors.[32,37,106] We show here that NLRC5 is also involved in the regulation of the PPARγ target FABP4. FABP4 is an intracellular lipid chaperone responsible for lipid storage, lipolysis and metabolism.[107–110] For *FABP4* induction, NLRC5 nuclear localization was needed and NLRC5 isoform 3 failed to mediate *FABP4* transcription, similar to what was observed earlier for NLRC5-mediated MHC class I gene expression,[37,85] rendering it likely that nuclear shuttling of NLRC5 is a prerequisite for the transcriptional activation of PPARγ targets. Of interest, there is independent evidence that NLRC5 is a potent transcriptional regulator beyond MHC class I genes.[78,111] In accordance with our data, Luan et al. showed reduced FABP4 and CD36 mRNA levels upon KD of *NLRC5* in human aortic smooth muscle cells (HASMC) and regulation of PPAR response element (PPRE) activity by NLRC5 in a HEK293 cell-based PPRE reporter gene assay.[78] This is in line with our hypothesis of a synergistic interplay between NLRC5 and PPARγ in the regulation of PPARγ targets, although in our case the regulation of CD36 by NLRC5 and PPARγ was only marginal (Figure 4C). NLRC5 has also been reported to regulate the transcription of butyrophilin (BTN) genes via an atypical S/X/Y module.[111] Most importantly, both studies provide evidence for a functional implication of the NLRC5-mediated regulation of non-MHC class I genes with NLRC5 via PPARγ activation alleviating vascular remodeling and neointima formation[78] and NLRC5-regulated BTN3A gene expression potentially aiding in anti-mycobacterial immunity.[111] Thus, it is likely that the synergistic regulation of PPARγ targets by PPARγ and NLRC5 observed by us is functionally connected to the obesity-phenotype we observe in *Nlrc5*$^{-/-}$ animals.

In agreement with published work[78] we show that PPARγ interacts with the NACHT domain of NLRC5. We further characterize this interaction by providing evidence that only PPARγ isoform 1, but not isoform 2, is binding to NLRC5. PPARγ2 differs from PPARγ1 only by possesing 28 additional N-terminal aminos acids.[63,73] Hence, it was unexpected that only the shorter PPARγ isoform interacts with NLRC5, especially taking into consideration that the binding site for NLRC5 has been mapped to the C-terminal ligand-binding domain (LBD) of PPARγ.[78] PPARγ ligand-binding has been shown to be regulated via intra-domain communications between the N-terminal domain and the LBD, and modifications of the PPARγ N-terminus result in altered ligand-binding affinity.[112] Recently, NLRC5 was proposed to be a PPARγ ligand.[78] Thus, differences in the isoforms' N-termini could explain the differential binding of NLRC5. We also observed the co-immunoprecipitation of CIITA, but not NOD1, with PPARγ1. CIITA, like

NLRC5, functions as a transcriptional activator, and is the master regulator of MHC class II genes.[79] Phylogenetically, CIITA is NLRC5's next closest relative, especially concerning the NACHT domain.[40] The fact that PPARγ1 did not associate with NOD1, which is NLRC5's next closest phylogenetic relative in the NACHT domain after CIITA,[40] highlights the high specificity of the PPARγ1:NLRC5 interaction. PPARγ has already been shown to immunoprecipitate with CIITA in the context of collagen synthesis[113] and furthermore to be recruited to the CIITA promoter IV[114] and to activate MHC class II genes.[113] Mechanistically, this opens up the possibility that PPARγ and NLRC5 function as a transcriptional complex, binding to the promoters of PPARγ target genes via PPARγ:PPRE interaction resulting in synergistic regulation of transcription.

NLRC5 confers its transcriptional activity as well as its specificity toward MHC class I genes via its N-terminal DD.[33] In this study we identify Sin3A and NELFB as two novel interactors of the transcriptionally active DD of NLRC5, with Sin3A silencing enhancing NLRC5-regulated *FABP4* transcription. Sin3A is primarily known as a transcriptional repressor by providing a scaffold for transcriptional complex formation, most prominently the Sin3-HDAC1/2 complex. Sin3A has no intrinsic DNA binding activity and thus needs the interaction with transcription factors, direct or via a third adaptor molecule, to be able to associate with the DNA.[89] Murine Sin3A has been shown to be recruited to the PPARγ promoter by TGF-β1 stimulation in the scenario of cardiac pressure overload, leading to PPARγ repression.[115] Of interest, Sin3A has also been shown to interact and thus help with the recruitment of HDACs to the two co-repressor complexes nuclear receptor co-repressor (NCoR) and silencing mediator of retinoic acid and thyroid hormone receptor (SMRT),[116–119] both known to associate with and mediate the transcriptional repression of type II nuclear hormone receptors, like PPARγ, in unliganded state[120] (reviewed in[121]). Upon ligand binding, the co-repressor complex is released and co-activators are recruited.[122,123]

Thus, a possible working hypothesis would be a "double" negative transcriptional regulation of PPARγ targets in the absence of ligands: Once by the binding of the long-known transcriptional co-repressor/Sin3A/HDAC complexes and once by Sin3A (via NLRC5's DD) binding to and mediating additional HDAC recruitment to the NLRC5:PPARγ complex sitting at the FABP4 promoter (Figure S7A). Although the classical co-repressor complexes are exchanged for co-activators on ligand-binding, the Sin3A/NLRC5 complex remains associated with PPARγ, thereby fine-tuning PPARγ target gene transcription (Figure S7B). This role of Sin3A in refining transcription would explain the moderate effect of Sin3A KD (Figure S7C) on *FABP4* transcription and the unchanged *HLA-A* levels on Sin3A silencing, as induction of MHC class I genes is saturated by NLRC5 expression, losing that moderating effect of Sin3A. In line with this working hypothesis, Sin3A has been shown to fine-tune the transcriptional response of the thyroid hormone (TH) receptor, also a type II nuclear hormone receptor, via interaction with a newly identified protein interacting with the DBD of the TH receptor.[124]

How exactly the synergistic regulation of FABP4 by NLRC5, PPARγ and eventually Sin3A is connected to the obesity-like phenotype of *Nlrc5*$^{-/-}$ animals on HFD remains to be clarified. Of interest, it has been shown that *Fabp4* deficient mice are protected against the development of diet-induced IR and impaired glucose tolerance albeit the development of more severe obesity, and that adipoyctes of *Fabp4*$^{-/-}$ animals present with reduced lipolysis efficiency.[125] In line, genetically obese mice (ob/ob mice) presented with significantly reduced blood glucose levels and insulin sensitivity upon genetic disruption of *Fabp4*, which was accompanied by higher body weight and reduced plasma triglyceride and cholesterol levels.[126] A more recent study demostrated that RNA interferance (RNAi)-mediated germline KD of *Fabp4* increased body weight and fat mass in diet-induced obesity mice, but did not affect plasma glucose and lipid homeostasis or insulin sensitivity.[127] These data undermine our working model of NLRC5 co-regulating *FABP4* transcription, with *NLRC5* deficiency leading to highly reduced *FABP4* transcription and thereby increased adipose tissues and adipocyte size (eventually because of defective adipocyte lipolysis) (Figure S7C), which is reflected in the higher body weight (Figure 1), but improvements in serum cholesterol and triglyceride levels (Figures S2A and S2B) in our *Nlrc5*$^{-/-}$ animals. As CD36 was also marginally upregulated in GFP-NLRC5 compared to GFP expressing cells (Figure 4C) and LPS-stimulated BMDMs from *Nlrc5*$^{-/-}$ mice responded less to PPARγ activation compared to WT cells (Figure S5), it is likely that also other PPARγ targets involved in metabolism and inflammation are co-regulated by NLRC5, with their dysfunctional regulation by *NLRC5* deficiency possibly also contributing to the here-described role of NLRC5 in HFD-induced obesity.

In summary, we show that *Nlrc5* deficiency in female mice under HFD leads to higher weight gain and more fat accumulation compared to WT animals. We further describe a synergistic regulation of the PPARγ

target FABP4 by PPARγ activation and NLRC5 expression and identify one of the two novel NLRC5 interaction partners, Sin3A, to be involved in this synergistic transcriptional regulation.

Limitations of the study

Limitations include the fact that a considerable part of the functional data was generated using human cell lines and ectopical expression of NLRC5. In the mouse model, the use of only one diet and the lack of conditional KO in particular cell types does not allow to draw conclusion on the cell types involved. Lastly, the relevance of our findings in humans remains to be elucidated.

STAR★METHODS

Detailed methods are provided in the online version of this paper and include the following:

- KEY RESOURCES TABLE
- RESOURCE AVAILABILITY
  - Lead contact
  - Materials availability
  - Data and code availability
- EXPERIMENTAL MODEL AND SUBJECT DETAILS
  - Mice
  - Cell culture
  - Generation and stimulation of bone marrow-derived macrophages
- METHOD DETAILS
  - Histology
  - Cholesterol and triglyceride measurement in serum
  - Taxonomic microbiota analysis
  - Plasmids and reagents
  - siRNA-mediated silencing
  - Co-immunoprecipitation
  - Immunoblotting
  - qRT-PCR
  - Indirect immunofluorescence
  - Measurement of cytokines
  - Luciferase reporter gene assays
  - Yeast two-hybrid screening
- QUANTIFICATION AND STATISTICAL ANALYSIS

SUPPLEMENTAL INFORMATION

Supplemental information can be found online at https://doi.org/10.1016/j.isci.2023.106313.

ACKNOWLEDGMENTS

We thank Yvonne Postma and Monika Schuhmacher for technical assistance with the experiments and Selina Briese for help with the mouse handling and Lucy Hezinger and Felix Biber for bioinformatic assistance. We acknowledge Prof. Subburaj Ilangumaran (University of Sherbrooke, QC, Canada) for helpful discussions. Funding: SB acknowledges support by the Landesgraduiertenförderung of Baden-Württemberg. SR acknowledges funding from Canadian Institutes of Health Research-CIHR- 202003PJT-437040. This project was supported by a mobility grant from the DAAD (PPP project 57599716).

AUTHOR CONTRIBUTIONS

S.B., V.A., I.K., A.M.B., and K.E. performed the experiments and analyzed the data. P.R. provided the *Nlrc5*$^{-/-}$ mice. F.R. and S.R. condcuted experiments with mice and provided input on the study design. S.B., V.A., A.M.B., W.F.F., and T.A.K. wrote the first draft of the manuscript and prepared the figures. A.M.B., M.S., and W.F.F. performed the micobiome analysis. T.A.K. conceptualized the study, analyzed the data and assured funding. All authors edited the final manuscript and approved the submitted version.

DECLARATION OF INTERESTS

The authors declare no competing interests.

Received: December 12, 2022
Revised: January 11, 2023
Accepted: February 27, 2023
Published: March 2, 2023

REFERENCES

1. Ng, M., Fleming, T., Robinson, M., Thomson, B., Graetz, N., Margono, C., Mullany, E.C., Biryukov, S., Abbafati, C., Abera, S.F., et al. (2014). Global, regional, and national prevalence of overweight and obesity in children and adults during 1980-2013: a systematic analysis for the Global Burden of Disease Study 2013. Lancet *384*, 766–781. https://doi.org/10.1016/S0140-6736(14)60460-8.

2. Eckel, R.H., Grundy, S.M., and Zimmet, P.Z. (2005). The metabolic syndrome. Lancet *365*, 1415–1428. https://doi.org/10.1016/S0140-6736(05)66378-7.

3. Hotamisligil, G.S., Shargill, N.S., and Spiegelman, B.M. (1993). Adipose expression of tumor necrosis factor-alpha: direct role in obesity-linked insulin resistance. Science *259*, 87–91. https://doi.org/10.1126/science.7678183.

4. Wellen, K.E., and Hotamisligil, G.S. (2005). Inflammation, stress, and diabetes. J. Clin. Invest. *115*, 1111–1119. https://doi.org/10.1172/JCI25102.

5. Olefsky, J.M., and Glass, C.K. (2010). Macrophages, inflammation, and insulin resistance. Annu. Rev. Physiol. *72*, 219–246. https://doi.org/10.1146/annurev-physiol-021909-135846.

6. Shoelson, S.E., Lee, J., and Yuan, M. (2003). Inflammation and the IKK beta/I kappa B/NF-kappa B axis in obesity- and diet-induced insulin resistance. Int. J. Obes. Relat. Metab. Disord. *27* (*Suppl 3*), S49–S52. https://doi.org/10.1038/sj.ijo.0802501.

7. Weisberg, S.P., McCann, D., Desai, M., Rosenbaum, M., Leibel, R.L., and Ferrante, A.W., Jr. (2003). Obesity is associated with macrophage accumulation in adipose tissue. J. Clin. Invest. *112*, 1796–1808. https://doi.org/10.1172/JCI19246.

8. Janeway, C.A., Jr., and Medzhitov, R. (2002). Innate immune recognition. Annu. Rev. Immunol. *20*, 197–216. https://doi.org/10.1146/annurev.immunol.20.083001.084359.

9. Matzinger, P. (2002). The danger model: a renewed sense of self. Science *296*, 301–305. https://doi.org/10.1126/science.1071059.

10. McLaughlin, T., Ackerman, S.E., Shen, L., and Engleman, E. (2017). Role of innate and adaptive immunity in obesity-associated metabolic disease. J. Clin. Invest. *127*, 5–13. https://doi.org/10.1172/JCI88876.

11. Shi, H., Kokoeva, M.V., Inouye, K., Tzameli, I., Yin, H., and Flier, J.S. (2006). TLR4 links innate immunity and fatty acid-induced insulin resistance. J. Clin. Invest. *116*, 3015–3025. https://doi.org/10.1172/JCI28898.

12. Arnold, C., Kienes, I., Sowa, A.S., and Kufer, T.A. (2018). NOD-Like ReceptorseLS (John Wiley & Sons, Ltd). https://doi.org/10.1002/9780470015902.a0026236.

13. Kim, Y.K., Shin, J.S., and Nahm, M.H. (2016). NOD-like receptors in infection, immunity, and diseases. Yonsei Med. J. *57*, 5–14. https://doi.org/10.3349/ymj.2016.57.1.5.

14. Mirza, N., Bauer, S., and Kufer, T.A. (2019). Angeborene immunität und adipositas – die rolle der nod-like-rezeptoren (NLR). Aktuel. Ernahrungsmed. *44*, 248–260. https://doi.org/10.1055/a-0918-5630.

15. Chan, K.L., Tam, T.H., Boroumand, P., Prescott, D., Costford, S.R., Escalante, N.K., Fine, N., Tu, Y., Robertson, S.J., Prabaharan, D., et al. (2017). Circulating NOD1 activators and hematopoietic NOD1 contribute to metabolic inflammation and insulin resistance. Cell Rep. *18*, 2415–2426. https://doi.org/10.1016/j.celrep.2017.02.027.

16. Schertzer, J.D., and Klip, A. (2011). Give a NOD to insulin resistance. Am. J. Physiol. Endocrinol. Metab. *301*, E585–E586. https://doi.org/10.1152/ajpendo.00362.2011.

17. Schertzer, J.D., Tamrakar, A.K., Magalhães, J.G., Pereira, S., Bilan, P.J., Fullerton, M.D., Liu, Z., Steinberg, G.R., Giacca, A., Philpott, D.J., and Klip, A. (2011). NOD1 activators link innate immunity to insulin resistance. Diabetes *60*, 2206–2215. https://doi.org/10.2337/db11-0004.

18. Shiny, A., Regin, B., Balachandar, V., Gokulakrishnan, K., Mohan, V., Babu, S., and Balasubramanyam, M. (2013). Convergence of innate immunity and insulin resistance as evidenced by increased nucleotide oligomerization domain (NOD) expression and signaling in monocytes from patients with type 2 diabetes. Cytokine *64*, 564–570. https://doi.org/10.1016/j.cyto.2013.08.003.

19. Lappas, M. (2014). NOD1 expression is increased in the adipose tissue of women with gestational diabetes. J. Endocrinol. *222*, 99–112. https://doi.org/10.1530/JOE-14-0179.

20. Zhou, Y.J., Liu, C., Li, C.L., Song, Y.L., Tang, Y.S., Zhou, H., Li, A., Li, Y., Weng, Y., and Zheng, F.P. (2015). Increased NOD1, but not NOD2, activity in subcutaneous adipose tissue from patients with metabolic syndrome. Obesity *23*, 1394–1400. https://doi.org/10.1002/oby.21113.

21. Stienstra, R., van Diepen, J.A., Tack, C.J., Zaki, M.H., van de Veerdonk, F.L., Perera, D., Neale, G.A., Hooiveld, G.J., Hijmans, A., Vroegrijk, I., et al. (2011). Inflammasome is a central player in the induction of obesity and insulin resistance. Proc. Natl. Acad. Sci. USA *108*, 15324–15329. https://doi.org/10.1073/pnas.1100255108.

22. Wen, H., Gris, D., Lei, Y., Jha, S., Zhang, L., Huang, M.T.H., Brickey, W.J., and Ting, J.P.Y. (2011). Fatty acid-induced NLRP3-ASC inflammasome activation interferes with insulin signaling. Nat. Immunol. *12*, 408–415. https://doi.org/10.1038/ni.2022.

23. Youm, Y.H., Adijiang, A., Vandanmagsar, B., Burk, D., Ravussin, A., and Dixit, V.D. (2011). Elimination of the NLRP3-ASC inflammasome protects against chronic obesity-induced pancreatic damage. Endocrinology *152*, 4039–4045. https://doi.org/10.1210/en.2011-1326.

24. Bando, S., Fukuda, D., Soeki, T., Nishimoto, S., Uematsu, E., Matsuura, T., Ise, T., Tobiume, T., Yamaguchi, K., Yagi, S., et al. (2015). Expression of NLRP3 in subcutaneous adipose tissue is associated with coronary atherosclerosis. Atherosclerosis *242*, 407–414. https://doi.org/10.1016/j.atherosclerosis.2015.07.043.

25. Esser, N., L'Homme, L., De Roover, A., Kohnen, L., Scheen, A.J., Moutschen, M., Piette, J., Legrand-Poels, S., and Paquot, N. (2013). Obesity phenotype is related to NLRP3 inflammasome activity and immunological profile of visceral adipose tissue. Diabetologia *56*, 2487–2497. https://doi.org/10.1007/s00125-013-3023-9.

26. Serena, C., Keiran, N., Ceperuelo-Mallafre, V., Ejarque, M., Fradera, R., Roche, K., Nuñez-Roa, C., Vendrell, J., and Fernández-Veledo, S. (2016). Obesity and type 2 diabetes alters the immune properties of human adipose derived stem cells. Stem Cell. *34*, 2559–2573. https://doi.org/10.1002/stem.2429.

27. Yin, Z., Deng, T., Peterson, L.E., Yu, R., Lin, J., Hamilton, D.J., Reardon, P.R., Sherman, V., Winnier, G.E., Zhan, M., et al. (2014). Transcriptome analysis of human adipocytes implicates the NOD-like receptor pathway in obesity-induced adipose inflammation. Mol. Cell. Endocrinol. *394*, 80–87. https://doi.org/10.1016/j.mce.2014.06.018.

28. Cavallari, J.F., Fullerton, M.D., Duggan, B.M., Foley, K.P., Denou, E., Smith, B.K., Desjardins, E.M., Henriksbo, B.D., Kim, K.J., Tuinema, B.R., et al. (2017). Muramyl dipeptide-based postbiotics mitigate obesity-induced insulin resistance via IRF4. Cell Metab. *25*, 1063–1074.e3. https://doi.org/10.1016/j.cmet.2017.03.021.

29. Denou, E., Lolmède, K., Garidou, L., Pomie, C., Chabo, C., Lau, T.C., Fullerton, M.D., Nigro, G., Zakaroff-Girard, A., Luche, E., et al. (2015). Defective NOD2 peptidoglycan sensing promotes diet-induced

inflammation, dysbiosis, and insulin resistance. EMBO Mol. Med. *7*, 259–274. https://doi.org/10.15252/emmm.201404169.

30. Rodriguez-Nunez, I., Caluag, T., Kirby, K., Rudick, C.N., Dziarski, R., and Gupta, D. (2017). Nod2 and Nod2-regulated microbiota protect BALB/c mice from diet-induced obesity and metabolic dysfunction. Sci. Rep. *7*, 548. https://doi.org/10.1038/s41598-017-00484-2.

31. Truax, A.D., Chen, L., Tam, J.W., Cheng, N., Guo, H., Koblansky, A.A., Chou, W.C., Wilson, J.E., Brickey, W.J., Petrucelli, A., et al. (2018). The inhibitory innate immune sensor NLRP12 maintains a threshold against obesity by regulating gut microbiota homeostasis. Cell Host Microbe *24*, 364–378.e6. https://doi.org/10.1016/j.chom.2018.08.009.

32. Meissner, T.B., Li, A., Biswas, A., Lee, K.H., Liu, Y.J., Bayir, E., Iliopoulos, D., van den Elsen, P.J., and Kobayashi, K.S. (2010). NLR family member NLRC5 is a transcriptional regulator of MHC class I genes. Proc. Natl. Acad. Sci. USA *107*, 13794–13799. https://doi.org/10.1073/pnas.1008684107.

33. Neerincx, A., Jakobshagen, K., Utermöhlen, O., Büning, H., Steimle, V., and Kufer, T.A. (2014). The N-terminal domain of NLRC5 confers transcriptional activity for MHC class I and II gene expression. J. Immunol. *193*, 3090–3100. https://doi.org/10.4049/jimmunol.1401065.

34. Neerincx, A., Lautz, K., Menning, M., Kremmer, E., Zigrino, P., Hösel, M., Büning, H., Schwarzenbacher, R., and Kufer, T.A. (2010). A role for the human nucleotide-binding domain, leucine-rich repeat-containing family member NLRC5 in antiviral responses. J. Biol. Chem. *285*, 26223–26232. https://doi.org/10.1074/jbc.M110.109736.

35. Benkő, S., Kovács, E.G., Hezel, F., and Kufer, T.A. (2017). NLRC5 functions beyond MHC I regulation-what do we know so far? Front. Immunol. *8*, 150. https://doi.org/10.3389/fimmu.2017.00150.

36. Meissner, T.B., Li, A., and Kobayashi, K.S. (2012). NLRC5: a newly discovered MHC class I transactivator (CITA). Microbes Infect. *14*, 477–484. https://doi.org/10.1016/j.micinf.2011.12.007.

37. Neerincx, A., Rodriguez, G.M., Steimle, V., and Kufer, T.A. (2012). NLRC5 controls basal MHC class I gene expression in an MHC enhanceosome-dependent manner. J. Immunol. *188*, 4940–4950. https://doi.org/10.4049/jimmunol.1103136.

38. Downs, I., Vijayan, S., Sidiq, T., and Kobayashi, K.S. (2016). CITA/NLRC5: a critical transcriptional regulator of MHC class I gene expression. Biofactors *42*, 349–357. https://doi.org/10.1002/biof.1285.

39. Meissner, T.B., Liu, Y.J., Lee, K.H., Li, A., Biswas, A., van Eggermond, M.C.J.A., van den Elsen, P.J., and Kobayashi, K.S. (2012). NLRC5 cooperates with the RFX transcription factor complex to induce MHC class I gene expression. J. Immunol. *188*, 4951–4958. https://doi.org/10.4049/jimmunol.1103160.

40. Benko, S., Magalhaes, J.G., Philpott, D.J., and Girardin, S.E. (2010). NLRC5 limits the activation of inflammatory pathways. J. Immunol. *185*, 1681–1691. https://doi.org/10.4049/jimmunol.0903900.

41. Cui, J., Zhu, L., Xia, X., Wang, H.Y., Legras, X., Hong, J., Ji, J., Shen, P., Zheng, S., Chen, Z.J., and Wang, R.F. (2010). NLRC5 negatively regulates the NF-kappaB and type I interferon signaling pathways. Cell *141*, 483–496. https://doi.org/10.1016/j.cell.2010.03.040.

42. Kumar, H., Pandey, S., Zou, J., Kumagai, Y., Takahashi, K., Akira, S., and Kawai, T. (2011). NLRC5 deficiency does not influence cytokine induction by virus and bacteria infections. J. Immunol. *186*, 994–1000. https://doi.org/10.4049/jimmunol.1002094.

43. Li, L., Xu, T., Huang, C., Peng, Y., and Li, J. (2014). NLRC5 mediates cytokine secretion in RAW264.7 macrophages and modulated by the JAK2/STAT3 pathway. Inflammation *37*, 835–847. https://doi.org/10.1007/s10753-013-9804-y.

44. Robbins, G.R., Truax, A.D., Davis, B.K., Zhang, L., Brickey, W.J., and Ting, J.P.Y. (2012). Regulation of class I major histocompatibility complex (MHC) by nucleotide-binding domain, leucine-rich repeat-containing (NLR) proteins. J. Biol. Chem. *287*, 24294–24303. https://doi.org/10.1074/jbc.M112.364604.

45. Tong, Y., Cui, J., Li, Q., Zou, J., Wang, H.Y., and Wang, R.F. (2012). Enhanced TLR-induced NF-kappaB signaling and type I interferon responses in NLRC5 deficient mice. Cell Res. *22*, 822–835. https://doi.org/10.1038/cr.2012.53.

46. Yao, Y., Wang, Y., Chen, F., Huang, Y., Zhu, S., Leng, Q., Wang, H., Shi, Y., and Qian, Y. (2012). NLRC5 regulates MHC class I antigen presentation in host defense against intracellular pathogens. Cell Res. *22*, 836–847. https://doi.org/10.1038/cr.2012.56.

47. Kuenzel, S., Till, A., Winkler, M., Häsler, R., Lipinski, S., Jung, S., Grötzinger, J., Fickenscher, H., Schreiber, S., and Rosenstiel, P. (2010). The nucleotide-binding oligomerization domain-like receptor NLRC5 is involved in IFN-dependent antiviral immune responses. J. Immunol. *184*, 1990–2000. https://doi.org/10.4049/jimmunol.0900557.

48. Wu, X.M., Hu, Y.W., Xue, N.N., Ren, S.S., Chen, S.N., Nie, P., and Chang, M.X. (2017). Role of zebrafish NLRC5 in antiviral response and transcriptional regulation of MHC related genes. Dev. Comp. Immunol. *68*, 58–68. https://doi.org/10.1016/j.dci.2016.11.018.

49. Chelbi, S.T., and Guarda, G. (2016). NLRC5, a promising new entry in tumor immunology. J. Immunother. Cancer *4*, 39. https://doi.org/10.1186/s40425-016-0143-z.

50. Ma, H.L., Zhao, X.F., Chen, G.Z., Fang, R.H., and Zhang, F.R. (2016). Silencing NLRC5 inhibits extracellular matrix expression in keloid fibroblasts via inhibition of transforming growth factor-beta1/Smad signaling pathway. Biomed. Pharmacother. *83*, 1016–1021. https://doi.org/10.1016/j.biopha.2016.08.012.

51. Peng, Y.Y., He, Y.H., Chen, C., Xu, T., Li, L., Ni, M.M., Meng, X.M., Huang, C., and Li, J. (2016). NLRC5 regulates cell proliferation, migration and invasion in hepatocellular carcinoma by targeting the Wnt/beta-catenin signaling pathway. Cancer Lett. *376*, 10–21. https://doi.org/10.1016/j.canlet.2016.03.006.

52. Staehli, F., Ludigs, K., Heinz, L.X., Seguín-Estévez, Q., Ferrero, I., Braun, M., Schroder, K., Rebsamen, M., Tardivel, A., Mattmann, C., et al. (2012). NLRC5 deficiency selectively impairs MHC class I- dependent lymphocyte killing by cytotoxic T cells. J. Immunol. *188*, 3820–3828. https://doi.org/10.4049/jimmunol.1102671.

53. Shukla, A., Cloutier, M., Appiya Santharam, M., Ramanathan, S., and Ilangumaran, S. (2021). The MHC class-I transactivator NLRC5: implications to cancer immunology and potential applications to cancer immunotherapy. Int. J. Mol. Sci. *22*, 1964. https://doi.org/10.3390/ijms22041964.

54. Davis, B.K., Roberts, R.A., Huang, M.T., Willingham, S.B., Conti, B.J., Brickey, W.J., Barker, B.R., Kwan, M., Taxman, D.J., Accavitti-Loper, M.A., et al. (2011). Cutting edge: NLRC5-dependent activation of the inflammasome. J. Immunol. *186*, 1333–1337. https://doi.org/10.4049/jimmunol.1003111.

55. Triantafilou, K., Kar, S., van Kuppeveld, F.J.M., and Triantafilou, M. (2013). Rhinovirus-induced calcium flux triggers NLRP3 and NLRC5 activation in bronchial cells. Am. J. Respir. Cell Mol. Biol. *49*, 923–934. https://doi.org/10.1165/rcmb.2013-0032OC.

56. Charlesworth, J.C., Peralta, J.M., Drigalenko, E., Göring, H.H., Almasy, L., Dyer, T.D., and Blangero, J. (2009). Toward the identification of causal genes in complex diseases: a gene-centric joint test of significance combining genomic and transcriptomic data. BMC Proc. *3* (*Suppl 7*), S92. https://doi.org/10.1186/1753-6561-3-s7-s92.

57. Hosseinzadeh, N., Mehrabi, Y., Daneshpour, M.S., Zayeri, F., Guity, K., and Azizi, F. (2019). Identifying new associated pleiotropic SNPs with lipids by simultaneous test of multiple longitudinal traits: an Iranian family-based study. Gene *692*, 156–169. https://doi.org/10.1016/j.gene.2019.01.007.

58. Lin, X., Peng, C., Greenbaum, J., Li, Z.F., Wu, K.H., Ao, Z.X., Zhang, T., Shen, J., and Deng, H.W. (2018). Identifying potentially common genes between dyslipidemia and osteoporosis using novel analytical approaches. Mol. Genet. Genom. *293*, 711–723. https://doi.org/10.1007/s00438-017-1414-1.

59. Meeks, K.A.C., Henneman, P., Venema, A., Burr, T., Galbete, C., Danquah, I., Schulze, M.B., Mockenhaupt, F.P., Owusu-Dabo, E., Rotimi, C.N., et al. (2017). An epigenome-wide association study in whole blood of measures of adiposity among Ghanaians: the RODAM study. Clin. Epigenet. *9*, 103. https://doi.org/10.1186/s13148-017-0403-x.

60. Luan, P., Zhuang, J., Zou, J., Li, H., Shuai, P., Xu, X., Zhao, Y., Kou, W., Ji, S., Peng, A., et al. (2018). NLRC5 deficiency ameliorates diabetic nephropathy through alleviating inflammation. FASEB J. *32*, 1070–1084. https://doi.org/10.1096/fj.201700511RR.

61. Ma, S.R., and Xie, X.W. (2017). NLRC5 deficiency promotes myocardial damage induced by high fat diet in mice through activating TLR4/NF-kappaB. Biomed. Pharmacother. *91*, 755–766. https://doi.org/10.1016/j.biopha.2017.03.062.

62. Tontonoz, P., and Spiegelman, B.M. (2008). Fat and beyond: the diverse biology of PPARgamma. Annu. Rev. Biochem. *77*, 289–312. https://doi.org/10.1146/annurev.biochem.77.061307.091829.

63. Janani, C., and Ranjitha Kumari, B.D. (2015). PPAR gamma gene–a review. Diabetes Metab. Syndr. *9*, 46–50. https://doi.org/10.1016/j.dsx.2014.09.015.

64. Tontonoz, P., Hu, E., and Spiegelman, B.M. (1994). Stimulation of adipogenesis in fibroblasts by PPAR gamma 2, a lipid-activated transcription factor. Cell *79*, 1147–1156. https://doi.org/10.1016/0092-8674(94)90006-x.

65. Barak, Y., Nelson, M.C., Ong, E.S., Jones, Y.Z., Ruiz-Lozano, P., Chien, K.R., Koder, A., and Evans, R.M. (1999). PPAR gamma is required for placental, cardiac, and adipose tissue development. Mol. Cell *4*, 585–595. https://doi.org/10.1016/s1097-2765(00)80209-9.

66. Rosen, E.D., Sarraf, P., Troy, A.E., Bradwin, G., Moore, K., Milstone, D.S., Spiegelman, B.M., and Mortensen, R.M. (1999). PPAR gamma is required for the differentiation of adipose tissue in vivo and in vitro. Mol. Cell *4*, 611–617. https://doi.org/10.1016/s1097-2765(00)80211-7.

67. Wang, F., Mullican, S.E., DiSpirito, J.R., Peed, L.C., and Lazar, M.A. (2013). Lipoatrophy and severe metabolic disturbance in mice with fat-specific deletion of PPARgamma. Proc. Natl. Acad. Sci. USA *110*, 18656–18661. https://doi.org/10.1073/pnas.1314863110.

68. Freedman, B.D., Lee, E.J., Park, Y., and Jameson, J.L. (2005). A dominant negative peroxisome proliferator-activated receptor-gamma knock-in mouse exhibits features of the metabolic syndrome. J. Biol. Chem. *280*, 17118–17125. https://doi.org/10.1074/jbc.M407539200.

69. He, W., Barak, Y., Hevener, A., Olson, P., Liao, D., Le, J., Nelson, M., Ong, E., Olefsky, J.M., and Evans, R.M. (2003). Adipose-specific peroxisome proliferator-activated receptor gamma knockout causes insulin resistance in fat and liver but not in muscle. Proc. Natl. Acad. Sci. USA *100*, 15712–15717. https://doi.org/10.1073/pnas.2536828100.

70. Barroso, I., Gurnell, M., Crowley, V.E., Agostini, M., Schwabe, J.W., Soos, M.A., Maslen, G.L., Williams, T.D., Lewis, H., Schafer, A.J., et al. (1999). Dominant negative mutations in human PPARgamma associated with severe insulin resistance, diabetes mellitus and hypertension. Nature *402*, 880–883. https://doi.org/10.1038/47254.

71. Savage, D.B., Tan, G.D., Acerini, C.L., Jebb, S.A., Agostini, M., Gurnell, M., Williams, R.L., Umpleby, A.M., Thomas, E.L., Bell, J.D., et al. (2003). Human metabolic syndrome resulting from dominant-negative mutations in the nuclear receptor peroxisome proliferator-activated receptor-gamma. Diabetes *52*, 910–917. https://doi.org/10.2337/diabetes.52.4.910.

72. Desvergne, B., and Wahli, W. (1999). Peroxisome proliferator-activated receptors: nuclear control of metabolism. Endocr. Rev. *20*, 649–688. https://doi.org/10.1210/edrv.20.5.0380.

73. Elbrecht, A., Chen, Y., Cullinan, C.A., Hayes, N., Leibowitz, M.D., Moller, D.E., and Berger, J. (1996). Molecular cloning, expression and characterization of human peroxisome proliferator activated receptors gamma 1 and gamma 2. Biochem. Biophys. Res. Commun. *224*, 431–437. https://doi.org/10.1006/bbrc.1996.1044.

74. Grygiel-Górniak, B. (2014). Peroxisome proliferator-activated receptors and their ligands: nutritional and clinical implications–a review. Nutr. J. *13*, 17. https://doi.org/10.1186/1475-2891-13-17.

75. Nakachi, Y., Yagi, K., Nikaido, I., Bono, H., Tonouchi, M., Schönbach, C., and Okazaki, Y. (2008). Identification of novel PPARgamma target genes by integrated analysis of ChIP-on-chip and microarray expression data during adipocyte differentiation. Biochem. Biophys. Res. Commun. *372*, 362–366. https://doi.org/10.1016/j.bbrc.2008.05.037.

76. Jenkins-Kruchten, A.E., Bennaars-Eiden, A., Ross, J.R., Shen, W.J., Kraemer, F.B., and Bernlohr, D.A. (2003). Fatty acid-binding protein-hormone-sensitive lipase interaction. Fatty acid dependence on binding. J. Biol. Chem. *278*, 47636–47643. https://doi.org/10.1074/jbc.M307680200.

77. Schroeder, F., Petrescu, A.D., Huang, H., Atshaves, B.P., McIntosh, A.L., Martin, G.G., Hostetler, H.A., Vespa, A., Landrock, D., Landrock, K.K., et al. (2008). Role of fatty acid binding proteins and long chain fatty acids in modulating nuclear receptors and gene transcription. Lipids *43*, 1–17. https://doi.org/10.1007/s11745-007-3111-z.

78. Luan, P., Jian, W., Xu, X., Kou, W., Yu, Q., Hu, H., Li, D., Wang, W., Feinberg, M.W., Zhuang, J., et al. (2019). NLRC5 inhibits neointima formation following vascular injury and directly interacts with PPARgamma. Nat. Commun. *10*, 2882. https://doi.org/10.1038/s41467-019-10784-y.

79. Steimle, V., Otten, L.A., Zufferey, M., and Mach, B. (1993). Complementation cloning of an MHC class II transactivator mutated in hereditary MHC class II deficiency (or bare lymphocyte syndrome). Cell *75*, 135–146.

80. Caruso, R., Warner, N., Inohara, N., and Núñez, G. (2014). NOD1 and NOD2: signaling, host defense, and inflammatory disease. Immunity *41*, 898–908. https://doi.org/10.1016/j.immuni.2014.12.010.

81. Vara, D., Morell, C., Rodríguez-Henche, N., and Diaz-Laviada, I. (2013). Involvement of PPARgamma in the antitumoral action of cannabinoids on hepatocellular carcinoma. Cell Death Dis. *4*, e618. https://doi.org/10.1038/cddis.2013.141.

82. Seimandi, M., Lemaire, G., Pillon, A., Perrin, A., Carlavan, I., Voegel, J.J., Vignon, F., Nicolas, J.C., and Balaguer, P. (2005). Differential responses of PPARalpha, PPARdelta, and PPARgamma reporter cell lines to selective PPAR synthetic ligands. Anal. Biochem. *344*, 8–15. https://doi.org/10.1016/j.ab.2005.06.010.

83. Akiyama, T.E., Baumann, C.T., Sakai, S., Hager, G.L., and Gonzalez, F.J. (2002). Selective intranuclear redistribution of PPAR isoforms by RXR alpha. Mol. Endocrinol. *16*, 707–721. https://doi.org/10.1210/mend.16.4.0797.

84. Umemoto, T., and Fujiki, Y. (2012). Ligand-dependent nucleo-cytoplasmic shuttling of peroxisome proliferator-activated receptors, PPARalpha and PPARgamma. Gene Cell. *17*, 576–596. https://doi.org/10.1111/j.1365-2443.2012.01607.x.

85. Meissner, T.B., Li, A., Liu, Y.J., Gagnon, E., and Kobayashi, K.S. (2012). The nucleotide-binding domain of NLRC5 is critical for nuclear import and transactivation activity. Biochem. Biophys. Res. Commun. *418*, 786–791. https://doi.org/10.1016/j.bbrc.2012.01.104.

86. Woster, A.P., and Combs, C.K. (2007). Differential ability of a thiazolidinedione PPARgamma agonist to attenuate cytokine secretion in primary microglia and macrophage-like cells. J. Neurochem. *103*, 67–76. https://doi.org/10.1111/j.1471-4159.2007.04706.x.

87. Bardelli, C., Amoruso, A., Federici Canova, D., Fresu, L., Balbo, P., Neri, T., Celi, A., and Brunelleschi, S. (2012). Autocrine activation of human monocyte/macrophages by monocyte-derived microparticles and modulation by PPARgamma ligands. Br. J. Pharmacol. *165*, 716–728. https://doi.org/10.1111/j.1476-5381.2011.01593.x.

88. Rain, J.C., Selig, L., De Reuse, H., Battaglia, V., Reverdy, C., Simon, S., Lenzen, G., Petel, F., Wojcik, J., Schächter, V., et al. (2001). The protein-protein interaction map of Helicobacter pylori. Nature *409*, 211–215. https://doi.org/10.1038/35051615.

89. Silverstein, R.A., and Ekwall, K. (2005). Sin3: a flexible regulator of global gene expression

and genome stability. Curr. Genet. *47*, 1–17. https://doi.org/10.1007/s00294-004-0541-5.

90. Nechaev, S., Fargo, D.C., dos Santos, G., Liu, L., Gao, Y., and Adelman, K. (2010). Global analysis of short RNAs reveals widespread promoter-proximal stalling and arrest of Pol II in Drosophila. Science *327*, 335–338. https://doi.org/10.1126/science.1181421.

91. Li, J., Liu, Y., Rhee, H.S., Ghosh, S.K.B., Bai, L., Pugh, B.F., and Gilmour, D.S. (2013). Kinetic competition between elongation rate and binding of NELF controls promoter-proximal pausing. Mol. Cell *50*, 711–722. https://doi.org/10.1016/j.molcel.2013.05.016.

92. Cao-Lei, L., Elgbeili, G., Szyf, M., Laplante, D.P., and King, S. (2019). Differential genome-wide DNA methylation patterns in childhood obesity. BMC Res. Notes *12*, 174. https://doi.org/10.1186/s13104-019-4189-0.

93. Moore, L.D., Le, T., and Fan, G. (2013). DNA methylation and its basic function. Neuropsychopharmacology *38*, 23–38. https://doi.org/10.1038/npp.2012.112.

94. Aslibekyan, S., Agha, G., Colicino, E., Do, A.N., Lahti, J., Ligthart, S., Marioni, R.E., Marzi, C., Mendelson, M.M., Tanaka, T., et al. (2018). Association of methylation signals with incident coronary heart disease in an epigenome-wide assessment of circulating tumor necrosis factor alpha. JAMA Cardiol. *3*, 463–472. https://doi.org/10.1001/jamacardio.2018.0510.

95. Daniel, H., Gholami, A.M., Berry, D., Desmarchelier, C., Hahne, H., Loh, G., Mondot, S., Lepage, P., Rothballer, M., Walker, A., et al. (2014). High-fat diet alters gut microbiota physiology in mice. ISME J. *8*, 295–308. https://doi.org/10.1038/ismej.2013.155.

96. Jo, J.K., Seo, S.H., Park, S.E., Kim, H.W., Kim, E.J., Kim, J.S., Pyo, J.Y., Cho, K.M., Kwon, S.J., Park, D.H., and Son, H.S. (2021). Gut microbiome and metabolome profiles associated with high-fat diet in mice. Metabolites *11*, 482. https://doi.org/10.3390/metabo11080482.

97. He, X., Zhang, M., Li, S.T., Li, X., Huang, Q., Zhang, K., Zheng, X., Xu, X.T., Zhao, D.G., and Ma, Y.Y. (2022). Alteration of gut microbiota in high-fat diet-induced obese mice using carnosic acid from rosemary. Food Sci. Nutr. *10*, 2325–2332. https://doi.org/10.1002/fsn3.2841.

98. Bailén, M., Bressa, C., Martínez-López, S., González-Soltero, R., Montalvo Lominchar, M.G., San Juan, C., and Larrosa, M. (2020). Microbiota features associated with a high-fat/low-fiber diet in healthy adults. Front. Nutr. *7*, 583608. https://doi.org/10.3389/fnut.2020.583608.

99. Bisanz, J.E., Upadhyay, V., Turnbaugh, J.A., Ly, K., and Turnbaugh, P.J. (2019). Meta-analysis reveals reproducible gut microbiome alterations in response to a high-fat diet. Cell Host Microbe *26*, 265–272.e4. https://doi.org/10.1016/j.chom.2019.06.013.

100. Li, H., Liu, F., Lu, J., Shi, J., Guan, J., Yan, F., Li, B., and Huo, G. (2020). Probiotic mixture of Lactobacillus plantarum strains improves lipid metabolism and gut microbiota structure in high fat diet-fed mice. Front. Microbiol. *11*, 512. https://doi.org/10.3389/fmicb.2020.00512.

101. Cui, H.X., Zhang, L.S., Luo, Y., Yuan, K., Huang, Z.Y., and Guo, Y. (2019). A purified anthraquinone-glycoside preparation from rhubarb ameliorates type 2 diabetes mellitus by modulating the gut microbiota and reducing inflammation. Front. Microbiol. *10*, 1423. https://doi.org/10.3389/fmicb.2019.01423.

102. Wang, Y., Qi, W., Song, G., Pang, S., Peng, Z., Li, Y., and Wang, P. (2020). High-fructose diet increases inflammatory cytokines and alters gut microbiota composition in rats. Mediators Inflamm. *2020*, 6672636. https://doi.org/10.1155/2020/6672636.

103. Guo, Z., Ali, Q., Abaidullah, M., Gao, Z., Diao, X., Liu, B., Wang, Z., Zhu, X., Cui, Y., Li, D., and Shi, Y. (2022). High fat diet-induced hyperlipidemia and tissue steatosis in rabbits through modulating ileal microbiota. Appl. Microbiol. Biotechnol. *106*, 7187–7207. https://doi.org/10.1007/s00253-022-12203-7.

104. Gloor, G.B., Wu, J.R., Pawlowsky-Glahn, V., and Egozcue, J.J. (2016). It's all relative: analyzing microbiome data as compositions. Ann. Epidemiol. *26*, 322–329. https://doi.org/10.1016/j.annepidem.2016.03.003.

105. Biswas, A., Meissner, T.B., Kawai, T., and Kobayashi, K.S. (2012). Cutting edge: impaired MHC class I expression in mice deficient for Nlrc5/class I transactivator. J. Immunol. *189*, 516–520. https://doi.org/10.4049/jimmunol.1200064.

106. Ludigs, K., Seguín-Estévez, Q., Lemeille, S., Ferrero, I., Rota, G., Chelbi, S., Mattmann, C., MacDonald, H.R., Reith, W., and Guarda, G. (2015). NLRC5 exclusively transactivates MHC class I and related genes through a distinctive SXY module. PLoS Genet. *11*, e1005088. https://doi.org/10.1371/journal.pgen.1005088.

107. Amiri, M., Yousefnia, S., Seyed Forootan, F., Peymani, M., Ghaedi, K., and Nasr Esfahani, M.H. (2018). Diverse roles of fatty acid binding proteins (FABPs) in development and pathogenesis of cancers. Gene *676*, 171–183. https://doi.org/10.1016/j.gene.2018.07.035.

108. Chmurzyńska, A. (2006). The multigene family of fatty acid-binding proteins (FABPs): function, structure and polymorphism. J. Appl. Genet. *47*, 39–48. https://doi.org/10.1007/BF03194597.

109. Hotamisligil, G.S., and Bernlohr, D.A. (2015). Metabolic functions of FABPs–mechanisms and therapeutic implications. Nat. Rev. Endocrinol. *11*, 592–605. https://doi.org/10.1038/nrendo.2015.122.

110. Lee, C.H., Lui, D.T.W., and Lam, K.S.L. (2021). Adipocyte fatty acid-binding protein, cardiovascular diseases and mortality. Front. Immunol. *12*, 589206. https://doi.org/10.3389/fimmu.2021.589206.

111. Dang, A.T., Strietz, J., Zenobi, A., Khameneh, H.J., Brandl, S.M., Lozza, L., Conradt, G., Kaufmann, S.H.E., Reith, W., Kwee, I., et al. (2021). NLRC5 promotes transcription of BTN3A1-3 genes and Vgamma9Vdelta2 T cell-mediated killing. iScience *24*, 101900. https://doi.org/10.1016/j.isci.2020.101900.

112. Shao, D., Rangwala, S.M., Bailey, S.T., Krakow, S.L., Reginato, M.J., and Lazar, M.A. (1998). Interdomain communication regulating ligand binding by PPAR-gamma. Nature *396*, 377–380. https://doi.org/10.1038/24634.

113. Xu, Y., Farmer, S.R., and Smith, B.D. (2007). Peroxisome proliferator-activated receptor gamma interacts with CIITA x RFX5 complex to repress type I collagen gene expression. J. Biol. Chem. *282*, 26046–26056. https://doi.org/10.1074/jbc.M703652200.

114. Kong, X., Fang, M., Fang, F., Li, P., and Xu, Y. (2009). PPARgamma enhances IFNgamma-mediated transcription and rescues the TGFbeta antagonism by stimulating CIITA in vascular smooth muscle cells. J. Mol. Cell. Cardiol. *46*, 748–757. https://doi.org/10.1016/j.yjmcc.2009.01.011.

115. Gong, K., Chen, M., Li, R., He, Y., Zhu, H., Yao, D., Oparil, S., and Zhang, Z. (2016). Smad3-mSin3A-HDAC1 complex is required for TGF-beta1-induced transcriptional inhibition of PPARgamma in mouse cardiac fibroblasts. Cell. Physiol. Biochem. *40*, 908–920. https://doi.org/10.1159/000453149.

116. Heinzel, T., Lavinsky, R.M., Mullen, T.M., Söderstrom, M., Laherty, C.D., Torchia, J., Yang, W.M., Brard, G., Ngo, S.D., Davie, J.R., et al. (1997). A complex containing N-CoR, mSin3 and histone deacetylase mediates transcriptional repression. Nature *387*, 43–48. https://doi.org/10.1038/387043a0.

117. Laherty, C.D., Yang, W.M., Sun, J.M., Davie, J.R., Seto, E., and Eisenman, R.N. (1997). Histone deacetylases associated with the mSin3 corepressor mediate mad transcriptional repression. Cell *89*, 349–356. https://doi.org/10.1016/s0092-8674(00)80215-9.

118. Nagy, L., Kao, H.Y., Chakravarti, D., Lin, R.J., Hassig, C.A., Ayer, D.E., Schreiber, S.L., and Evans, R.M. (1997). Nuclear receptor repression mediated by a complex containing SMRT, mSin3A, and histone deacetylase. Cell *89*, 373–380. https://doi.org/10.1016/s0092-8674(00)80218-4.

119. Wen, Y.D., Perissi, V., Staszewski, L.M., Yang, W.M., Krones, A., Glass, C.K., Rosenfeld, M.G., and Seto, E. (2000). The histone deacetylase-3 complex contains nuclear receptor corepressors. Proc. Natl. Acad. Sci. USA *97*, 7202–7207. https://doi.org/10.1073/pnas.97.13.7202.

120. Yu, C., Markan, K., Temple, K.A., Deplewski, D., Brady, M.J., and Cohen, R.N. (2005). The nuclear receptor corepressors NCoR and

SMRT decrease peroxisome proliferator-activated receptor gamma transcriptional activity and repress 3T3-L1 adipogenesis. J. Biol. Chem. *280*, 13600–13605. https://doi.org/10.1074/jbc.M409468200.

121. Feige, J.N., and Auwerx, J. (2007). Transcriptional coregulators in the control of energy homeostasis. Trends Cell Biol. *17*, 292–301. https://doi.org/10.1016/j.tcb.2007.04.001.

122. Lehrke, M., and Lazar, M.A. (2005). The many faces of PPARgamma. Cell *123*, 993–999. https://doi.org/10.1016/j.cell.2005.11.026.

123. McKenna, N.J., and O'Malley, B.W. (2002). Combinatorial control of gene expression by nuclear receptors and coregulators. Cell *108*, 465–474. https://doi.org/10.1016/s0092-8674(02)00641-4.

124. Mathur, M., Tucker, P.W., and Samuels, H.H. (2001). PSF is a novel corepressor that mediates its effect through Sin3A and the DNA binding domain of nuclear hormone receptors. Mol. Cell Biol. *21*, 2298–2311. https://doi.org/10.1128/MCB.21.7.2298-2311.2001.

125. Hotamisligil, G.S., Johnson, R.S., Distel, R.J., Ellis, R., Papaioannou, V.E., and Spiegelman, B.M. (1996). Uncoupling of obesity from insulin resistance through a targeted mutation in aP2, the adipocyte fatty acid binding protein. Science *274*, 1377–1379. https://doi.org/10.1126/science.274.5291.1377.

126. Uysal, K.T., Scheja, L., Wiesbrock, S.M., Bonner-Weir, S., and Hotamisligil, G.S. (2000). Improved glucose and lipid metabolism in genetically obese mice lacking aP2. Endocrinology *141*, 3388–3396. https://doi.org/10.1210/endo.141.9.7637.

127. Yang, R., Castriota, G., Chen, Y., Cleary, M.A., Ellsworth, K., Shin, M.K., Tran, J.L., Vogt, T.F., Wu, M., Xu, S., et al. (2011). RNAi-mediated germline knockdown of FABP4 increases body weight but does not improve the deranged nutrient metabolism of diet-induced obese mice. Int. J. Obes. *35*, 217–225. https://doi.org/10.1038/ijo.2010.128.

128. Kufer, T.A., Kremmer, E., Adam, A.C., Philpott, D.J., and Sansonetti, P.J. (2008). The pattern-recognition molecule Nod1 is localized at the plasma membrane at sites of bacterial interaction. Cell Microbiol. *10*, 477–486. https://doi.org/10.1111/j.1462-5822.2007.01062.x.

129. Tachibana, K., Kobayashi, Y., Tanaka, T., Tagami, M., Sugiyama, A., Katayama, T., Ueda, C., Yamasaki, D., Ishimoto, K., Sumitomo, M., et al. (2005). Gene expression profiling of potential peroxisome proliferator-activated receptor (PPAR) target genes in human hepatoblastoma cell lines inducibly expressing different PPAR isoforms. Nucl. Recept. *3*, 3. https://doi.org/10.1186/1478-1336-3-3.

130. Tanaka, T., Takeno, T., Watanabe, Y., Uchiyama, Y., Murakami, T., Yamashita, H., Suzuki, A., Aoi, R., Iwanari, H., Jiang, S.Y., et al. (2002). The generation of monoclonal antibodies against human peroxisome proliferator-activated receptors (PPARs). J. Atheroscler. Thromb. *9*, 233–242. https://doi.org/10.5551/jat.9.233.

131. Bolyen, E., Rideout, J.R., Dillon, M.R., Bokulich, N.A., Abnet, C.C., Al-Ghalith, G.A., Alexander, H., Alm, E.J., Arumugam, M., Asnicar, F., et al. (2019). Reproducible, interactive, scalable and extensible microbiome data science using QIIME 2. Nat. Biotechnol. *37*, 852–857. https://doi.org/10.1038/s41587-019-0209-9.

132. Glastonbury, C.A., Pulit, S.L., Honecker, J., Censin, J.C., Laber, S., Yaghootkar, H., Rahmioglu, N., Pastel, E., Kos, K., Pitt, A., et al. (2020). Machine Learning based histology phenotyping to investigate the epidemiologic and genetic basis of adipocyte morphology and cardiometabolic traits. PLoS Comput. Biol. *16*, e1008044. https://doi.org/10.1371/journal.pcbi.1008044.

133. Schindelin, J., Arganda-Carreras, I., Frise, E., Kaynig, V., Longair, M., Pietzsch, T., Preibisch, S., Rueden, C., Saalfeld, S., Schmid, B., et al. (2012). Fiji: an open-source platform for biological-image analysis. Nat. Methods *9*, 676–682. https://doi.org/10.1038/nmeth.2019.

134. Galarraga, M., Campión, J., Muñoz-Barrutia, A., Boqué, N., Moreno, H., Martínez, J.A., Milagro, F., and Ortiz-de-Solórzano, C. (2012). Adiposoft: automated software for the analysis of white adipose tissue cellularity in histological sections. J. Lipid Res. *53*, 2791–2796. https://doi.org/10.1194/jlr.D023788.

135. Abele, J., and Khayam-Bashi, H. (1979). Aqueous primary standard for use in measuring cholesterol by the cholesterol oxidase method. Clin. Chem. *25*, 132–135.

136. Callahan, B.J., McMurdie, P.J., Rosen, M.J., Han, A.W., Johnson, A.J.A., and Holmes, S.P. (2016). DADA2: high-resolution sample inference from Illumina amplicon data. Nat. Methods *13*, 581–583. https://doi.org/10.1038/nmeth.3869.

137. Quast, C., Pruesse, E., Yilmaz, P., Gerken, J., Schweer, T., Yarza, P., Peplies, J., and Glöckner, F.O. (2013). The SILVA ribosomal RNA gene database project: improved data processing and web-based tools. Nucleic Acids Res. *41*, D590–D596. https://doi.org/10.1093/nar/gks1219.

138. Schnappauf, F., Hake, S.B., Camacho Carvajal, M.M., Bontron, S., Lisowska-Grospierre, B., and Steimle, V. (2003). N-terminal destruction signals lead to rapid degradation of the major histocompatibility complex class II transactivator CIITA. Eur. J. Immunol. *33*, 2337–2347. https://doi.org/10.1002/eji.200323490.

139. Solaimani, P., Wang, F., and Hankinson, O. (2014). SIN3A, generally regarded as a transcriptional repressor, is required for induction of gene transcription by the aryl hydrocarbon receptor. J. Biol. Chem. *289*, 33655–33662. https://doi.org/10.1074/jbc.M114.611236.

140. Almeida-Oliveira, F., Leandro, J.G.B., Ausina, P., Sola-Penna, M., and Majerowicz, D. (2017). Reference genes for quantitative PCR in the adipose tissue of mice with metabolic disease. Biomed. Pharmacother. *88*, 948–955. https://doi.org/10.1016/j.biopha.2017.01.091.

141. El Maassarani, M., Barbarin, A., Fromont, G., Kaissi, O., Lebbe, M., Vannier, B., Moussa, A., and Séité, P. (2016). Integrated and functional genomics analysis validates the relevance of the nuclear variant ErbB380kDa in prostate cancer progression. PLoS One *11*, e0155950. https://doi.org/10.1371/journal.pone.0155950.

142. Formstecher, E., Aresta, S., Collura, V., Hamburger, A., Meil, A., Trehin, A., Reverdy, C., Betin, V., Maire, S., Brun, C., et al. (2005). Protein interaction mapping: a Drosophila case study. Genome Res. *15*, 376–384. https://doi.org/10.1101/gr.2659105.

STAR★METHODS

KEY RESOURCES TABLE

REAGENT or RESOURCE	SOURCE	IDENTIFIER
Antibodies		
Rabbit monoclonal anti-PPARγ	Cell Signaling	Cat#2443; RRID: AB_823598
Mouse monoclonal anti-GFP	Roche	Cat#11814460001; RRID: AB_390913
Mouse monoclonal anti-FLAG	Sigma-Aldrich	Cat# F3165; RRID: AB_259529
Mouse monoclonal anti-myc	Sigma-Aldrich	Cat# M4439; RRID: AB_439694
Mouse monoclonal anti-HLA-B	Santa Cruz	Cat#sc-55582; RRID: AB_831547
Rabbit polyclonal anti-GAPDH	Santa Cruz	Cat#sc-25778; RRID: AB_10167668
Mouse monoclonal anti-HLA-B/C	Kind gift from Victor Steimle, University of Sherbrooke, Canada	N/A
Goat anti-mouse IgG HRP conjugate	BioRad	Cat#170-6516; RRID: AB_11125547
Goat anti-rabbit IgG HRP conjugate	BioRad	Cat#170-6515; RRID: AB_11125142
Goat anti-mouse light chain specific HRP conjugate	Jackson ImmunoResearch	Cat#115-035-174; RRID: AB_2338512
Chemicals, peptides, and recombinant proteins		
Rosiglitazone	Sigma-Aldrich	Cat#R2408
GW9662	Sigma-Aldrich	Cat#M6191
Lipopolysaccharide (LPS)	InvivoGen	Cat#tlrl-peklps
HiPerFect transfection reagent	Qiagen	Cat#301705
Lipofectamine 2000	Thermo Fisher Scientific	Cat#10696153
XtremeGene 9	Sigma-Aldrich	Cat# 6365787001
Hoechst 33258	Sigma-Aldrich	Cat#861405
cOmplete Mini Protease Inhibitor Cocktail	Roche	Cat# 11836170001
2xKAPA2G Fast HotStart Genotyping Mix	KAPA Biosystems	Cat#KK5621
GFP-Trap Agarose resin	Chromotek	Cat#gta
Anti-FLAG M2 affinity gel	Sigma-Aldrich	Cat#A2220
Clarity Western ECL Substrate	BioRad	Cat#1705061
SuperSignal™ West Femto Maximum Sensitivity Substrate	Thermo Fisher Scientific	Cat#34094
Roti®-Histol	Carl Roth	Cat#6640.2
Hematoxylin	Sigma-Aldrich	Cat#GHS316
Eosin	Sigma-Aldrich	Cat#HT110116
Entallan®	Sigma-Aldrich	Cat#107960
Infinity™ Cholesterol Liquid Stable Reagent	Thermo Fisher Scientific	Cat#TR13421
Infinity™ Triglycerides Liquid Stable Reagent	Thermo Fisher Scientific	Cat#TR22421
Glycerol Standard Solution	Sigma-Aldrich	Cat#G7793
iQ SYBR Green Supermix	BioRad	Cat#1708880
GreenMasterMix	Genaxxon	Cat#M3023.0100
Critical commercial assays		
DNeasy Blood & Tissue Kit	Qiagen	Cat#69504
iScript cDNA synthesis Kit	BioRad	Cat#1708890
TNF-α ELISA	R&D Systems	Cat#DY410

(*Continued on next page*)

Continued

REAGENT or RESOURCE	SOURCE	IDENTIFIER
Fecal DNA Miniprep Kit	Zymo Research	Cat#D6010
Quick-16S NGS Library Prep Kit	Zymo Research	Cat#D6400
RNeasy Plus Mini Kit	Qiagen	Cat#74134
RNeasy Plus Universal Mini Kit	Qiagen	Cat#73404
Deposited data		
Nlrc5 WT and KO fecal microbiome sequence data	This paper	ENA at EMBL-EBI : PRJEB57871
Experimental models: Cell lines		
HEK293T cells	ATCC	Cat#CRL-3216; RRID: CVCL_0063
HeLa GFP	This paper	N/A
HeLa GFP-NLRC5	This paper	N/A
HeLa GFP-NLRC5 Isoform 3	This paper	N/A
HeLa GFP-NLRC5 NLS I	This paper	N/A
HeLa GFP-NLRC5 2xNLS	This paper	N/A
Experimental models: Organisms/strains		
Mouse C57BL/6J *Nlrc5*$^{-/-}$	Generated by GenOway	Philip Rosenstiel, University of Kiel, Germany
Oligonucleotides		
For genotyping primer sequences, please see section "mice" in STAR Methods	This paper	N/A
For qRT-PCR primer sequences please see section "qRT-PCR" in STAR Methods	This paper, if not stated otherwise	N/A
siRNA targeting hSin3A, siSin3A_5	Qiagen	SI02781240
siRNA targeting hSin3A, siSin3A_6	Qiagen	SI03047611
siRNA targeting hCOBRA1_7	Qiagen	SI04347854
Non-targeting siRNA control, AllStars Negative Control siRNA	Qiagen	SI03650318
Recombinant DNA		
Plasmid: GFP-NLRC5	Neerincx et al.[37]	N/A
Plasmid: FLAG-NLRC5	Neerincx et al.[34]	Addgene #37521; RRID: Addgene_37521
Plasmid: FLAG-NLRC5 Iso3	Neerincx et al.[34]	N/A
Plasmid: FLAG-NOD1	Kufer et al.[128]	N/A
Plasmid: PPARγ1	Tachibana et al.,[129] Tanaka et al.[130]	N/A
Plasmid: PPARγ2	Tachibana et al.,[129] Tanaka et al.[130]	N/A
Plasmid: FLAG-NLRC5 LRR	This paper	N/A
Plasmid: FLAG-NLRC5 DD	This paper	N/A
Plasmid: FLAG-NLRC5ΔDD	This paper	N/A
Plasmid: FLAG-CIITA	This paper	N/A
Plasmid: myc-NLRC5	Neerincx et al.[37]	N/A
Plasmid: myc-NLRC5 Iso3	Neerincx et al.[37]	N/A
Plasmid: myc-NLRC5 DD	Neerincx et al.[37]	N/A
Plasmid: myc-NLRC5ΔDD	Neerincx et al.[37]	N/A
Plasmid: FLAG-Sin3A	This paper	N/A
Plasmid: FLAG-NELFB	Kind gift from Patrick Mehlen, Research Cancer Center of Lyon	N/A

(*Continued on next page*)

Continued

REAGENT or RESOURCE	SOURCE	IDENTIFIER
Plasmid: HLA-B250 luciferase construct	Neerincx et al.[37]	N/A
Plasmid: β-galactosidase	Neerincx et al.[37]	N/A
Software and algorithms		
Leica LasX software	Leica	RRID: SCR_013673
Fijii	NIH	RRID: SCR_002285
GraphPad Prism	N/A	RRID: SCR_002798
R (v3.6.1)	N/A	RRID: SCR_001905
QIIME2 v 2019.7	Bolyen et al.[131]	RRID: SCR_018074
Adipocyte U-NET	Glastonurry et al.[132]	N/A
Other		
Microtainer® SST™ tubes	BD Medical	Cat#BDAM367953
Lysing Matrix D 2 mL tubes	MP Biomedicals	Cat#SGD135.55
Low-fat control diet	SNIFF	Cat#E15000
High-fat diet	SNIFF	Cat#E15186

RESOURCE AVAILABILITY

Lead contact

Further information and requests for resources and reagents should be directed to and will be fulfilled by the lead contact, Thomas A. Kufer (thomas.kufer@uni-hohenheim.de).

Materials availability

Cell lines and plasmids generated in this study are available upon request.

Data and code availability

The microbiome sequence data has been deposited at the European Nucleotide Archive (ENA) at EMBL-EBI and is publicly available as of the date of publication. The accession number is listed in the key resources table.

This paper does not report original code.

Any additional information required to reanalyse the data reported in this paper is available from the lead contact upon request.

EXPERIMENTAL MODEL AND SUBJECT DETAILS

Mice

Nlrc5$^{+/+}$ (Nlrc5 WT) and *Nlrc5*$^{-/-}$ mice in C57BL/6N background were kindly provided by Philip Rosenstiel (University of Kiel). Knockout mice (B6.129Sv/Pas-Nlrc5tm1) were generated by GenOway. *Nlrc5* was targeted in 129SvPas embryonic stem cells that were injected into a blastocyst of a C57BL/6J mouse. A targeting vector was designed in which exons 4–7 were replaced by a loxP-flanked neomycin resistance cassette. Chimeric animals were mated to C57BL/6J mice. The *Nlrc5* knockout mice were finally back crossed on C57BL/6N background (B6.129Sv/Pas-Nlrc5tm1geno). Genotyping was performed by Endpoint PCR using DNA isolated from tail tips. DNA was extracted using the DNeasy Blood & Tissue Kit (Qiagen) according to manufacturer's instructions. For Endpoint PCR, 2xKAPA2G Fast HotStart Genotyping Mix (KAPA Biosystems) and the following oligos were used: *Nlrc5* ko fwd, GCCAGACAGCATAGACCAGATAGTGG; *Nlrc5* ko rev, CTACTTCCATTTGTCACGTCCTGCACG; *Nlrc5* wt fwd, GAGTCACTCACTCTCCAGGGAC AGTGG; *Nlrc5* wt rev, CTGTTGAGCTGACGGTGGATGACC (Figure S1). Mice were imported by embryo transfer into the SPF containment at the central animal facility of the University of Hohenheim and KO and WT littermates were outcrossed on a C57BL/6N background. Animals were started on experimental diet at the age of 8 weeks. For the experiment, mice were kept in the working area of the central animal

facility of the University of Hohenheim. WT and *Nlrc5*$^{-/-}$ mice were not co-housed. All mice were fed a synthetic low-fat control diet (SNIFF, E15000) *ad libitum* for 1 week to adapt the mice to the diet. Afterwards, *Nlrc5* WT and KO mice were randomly distributed on the intervention groups (n = 5), either receiving the low-fat control diet or a synthetic high-fat diet containing 30% crude fat (SNIFF, E15186) (for detailed diet composition see Table S1). Mice were fed *ad libitum* for a total of 11 weeks and were weighted twice a week. Food uptake was determined once a week by back weighting the remaining food in each cage. Mice were kept in a 12 h light/dark cycle. Mice were dissected directly after sacrifice by CO_2 inhalation and blood collection by heart puncture. Tissues for RNA isolation were snap-frozen in liquid nitrogen and stored at −80°C until use. Tissues for histology were put in tissue embedding cassettes and maintained in 4% PFA at 4°C overnight before being dehydrated in an ascending ethanol series and paraffin-embedded using the Leica TP1020 automatic benchtop tissue processor (Leica). The use of mice and all following treatments were performed according to FELASA and institutional guidelines and were approved by the local authorities of the state of Baden-Württemberg, in accordance with the animal protection law of Germany, under the license number V347/18 EM, 35-9185.81/0469 and are described in the NTP 00024601-1-4.

Cell culture

HEK293T cells (ATCC, CRL-3216) were grown in DMEM supplemented with 10% heat-inactivated FBS. Stable, inducible cell lines expressing GFP-NLRC5 or GFP-NLRC5 mutants were generated by co-transfection of pOG44 and pcDNA5/FRT/TO-GFP-NLRC5, pcDNA5/FRT/TO-GFP-NLRC5 NLS I, pcDNA5/FRT/TO-GFP-NLRC5 2xNLS or pcDNA/FRT/TO-GFP-NLRC5 Iso3 into HeLa Flp-In T-REx cells (kindly provided by the Hentze Lab, EMBL Heidelberg) or Flp-In T-REx HEK293 (Invitrogen/Thermo Fischer Scientific, R78007) using Lipofectamine 2000 (Thermo Fisher Scientific). Transfectants were selected with 10 μg/mL blasticidin and 100 μg/mL (HEK) or 600 μg/mL (HeLa) hygromycin. Single clones were selected and characterized for inducible and uniform expression. Target gene expression was induced by 1 μg/mL doxycycline for at least 20 h prior to further experiments. Stable cell lines were grown in DMEM supplemented with 10% heat-inactivated FBS. All cell culture media were supplemented with penicillin and streptomycin. Where indicated, cells were treated with the indicated concentrations of rosiglitazone (Sigma-Aldrich) or 10 μM GW9662 (Sigma-Aldrich). Cells were routinely monitored for the absence of mycoplasma infection by PCR.

Generation and stimulation of bone marrow-derived macrophages

Bone marrow cells were isolated from the respective animal and cultured in DMEM supplemented with 5% heat-inactivated FBS, 1% penicillin and streptomycin, 1 mM sodium pyruvate, 1% non-essential amino acids, 50 μM β-mercaptoethanol and 30% L929 cell supernatant. Fresh L929 cell supernatant was added once (day 3) and bone marrow-derived macrophages were harvested after 6 days. When indicated, cells were activated overnight with 0.4 μg/mL rosiglitazone (Sigma-Aldrich) and stimulated with 50 ng/mL LPS (InvivoGen) for 6 h the next day.

METHOD DETAILS

Histology

Histological analysis was performed on 5 μm paraffin sections of mouse epididymal adipose tissue. Paraffin sections were de-paraffinated with Roti®-Histol (Carl Roth) and rehydrated in ethanol baths with decreasing concentrations (100–30%). After washing with ultrapure water, Hematoxylin (Sigma-Aldrich) was applied for 3 sec. Tissue was dehydrated by ethanol baths (75% and 85%) before Eosin (Sigma-Aldrich) was applied for 3 sec. Tissue was further dehydrated by short baths in ethanol (95% and 100%), then treated with Roti®-Histol and fixed with Entallan®. Stained sections were imaged using a Leica DMi8 microscope with a HC PL Fluotar L 20x/0.40 objective and processed using the Leica LasX software and Fijii.[133] For determination of adipocyte diameter, Fijii with the PlugIn Adiposoft[134] was used. For determination of adipocyte area, the deep learning-based method Adipocyte U-Net[132] was used as published, except for setting the threshold for segmentation to 0.5 and excluding cells cut off by the picture frame.

Cholesterol and triglyceride measurement in serum

Blood was obtained by heart puncture directly after sacrifice. Serum was obtained by incubating the blood for 3 to 4 h in Microtainer® SST™ tubes (BD Medical), followed by centrifugation at 6,000 x g for 8 min. Serum cholesterol and triglyceride concentrations were determined using the Infinity™ Triglycerides Liquid

Stable Reagent and the Infinity™ Cholesterol Liquid Stable Reagent (Thermo Fisher Scientific). As standard, a 500 mg/dL cholesterol solution prepared according to Abele and Khayam-Bashi[135] for cholesterol measurements and a glycerol standard solution of 2.5 mg/mL equivalent triolein concentration (Sigma-Aldrich) for triglyceride measurements were used. Standards were prepared by 1:2 serial dilutions, the highest standard being 500 mg/dL. 2 μL of standard solution or mouse serum were incubated for 15 min at 37°C with 200 μL Infinity™ Triglycerides or Infinity™ Cholesterol Liquid Stable Reagent in a 96-well plate format. Standards and samples were run in duplicates. Absorbance was measured at 540 nm, with a reference wavelength of 660 nm. A standard curve was generated, and the serum cholesterol and triglyceride concentrations of the individual samples were calculated.

Taxonomic microbiota analysis

Mouse faeces were collected on three consecutive days in week 1, weekly in week 3, 6 and 9, and on two days in week 11. Fecal samples were snap-frozen in liquid nitrogen immediately after collection and stored at −150°C.

Metagenomic DNA was extracted via mechanical lysis by bead beating in 700 μL lysis buffer (Zymo Research) for 40 seconds at 6 m/s in MP lysing matrix B tubes (0.1 mm silica spheres, MP Biomedicals). Subsequently, the DNA was purified and eluted in 100 μL RNase-free water using the ZR Fecal DNA Miniprep Kit (Zymo Research) according to the manufacturer's protocol.

The 16S rRNA gene region V3-V4 was amplified and prepared for sequencing with the Quick-16S NGS Library Prep Kit (Zymo Research) according to the manufacturer's recommendations. The pooled and normalized library was sequenced on an Illumina MiSeq Instrument (MiSeq Reagent Kit v3, 600 cycles, Illumina) at the University of Hohenheim, Stuttgart, Germany.

The processing of raw sequences was carried out with QIIME2 v 2019.7[131] comprising the denoising of data with the DADA2 plugin,[136] adapter trimming and chimera checking. Amplicon sequence variants (ASV) with less than 100 sequence reads were considered sequencing artifacts and excluded from subsequent analyses resulting in a total of 5.26 million reads. The sequencing depth was rarefied to 15,203 reads per sample and the taxonomic composition determined via mapping ASV sequences to the Silva Database.[137] The sequence data has been deposited at the European Nucleotide Archive (ENA) at EMBL-EBI under accession number PRJEB57871 (ENA: PRJEB57871) and is publicly available. Statistical analyses and data visualizations of the microbiome data were carried out using R (v3.6.1) and the packages vegan, biomformat, phyloseq, moments, nortest, lmerTest, emmeans, sjPlot and ComplexHeatmap. Anderson-Darling and Shapiro-Wilks tests were used to test for normal distribution of microbiota related parameters. As non-normal distribution was confirmed, non-parametric tests like the Wilcoxon rank-sum test (WRST) were used for group comparisons followed by Benjamini-Hochberg (BH) false discovery rate correction (FDR) when multiple testing was applied. Associations between the taxonomic microbiota composition with the dietary intervention or genotype were assessed via Generalized Linear Mixed Models (GLMMs). Only taxa with a relative abundance of > 0.001%, which were found in at least two samples, were included. A pseudocount of 1 was added to all samples to replace zero counts and the resulting relative abundances centered-log ratio-transformed. Associations of each relative taxon abundance with fixed effects including the dietary intervention (d), genotype (g), the interaction between both effects (d:g), and controls, i.e. the amplification plate batch effects, were assessed, while adjusting the model for repeated sampling within individuals and litter mates as random effects. Model fits were verified using diagnostic plots, estimated marginal means (EMMs) of subgroups compared by Tukey's Test and p-values adjusted using the BH procedure across all taxa. Significance thresholds were chosen as follows: $q \geq 0.05$ not significant, $q < 0.05$ *, $q < 0.01$ ** and $q < 0.001$ ***. Odds ratios (OR) with 95% likelihood-based confidence intervals (CI), as well as marginal and conditional R2 were calculated and reported for all significant models.

Plasmids and reagents

GFP-NLRC5,[37] FLAG-NLRC5 FL (Addgene #37521) and FLAG-NLRC5 Iso3[34] and FLAG-NOD1[128] have been described previously. Expression plasmids for PPARγ1 and PPARγ2 have been described[129,130] and were a kind gift from Oliver Burk (Dr. Margarete Fischer-Bosch Institute of Clinical Pharmacology, Stuttgart). FLAG-NLRC5 LRR, FLAG-NLRC5 DD and FLAG-NLRC5ΔDD were generated by molecular cloning of NLRC5 myc-tagged vectors[37] into pCMV-Tag2B vector (Stratagene). FLAG-CIITA was generated by

molecular cloning from EBS-NPL-CIITA-FIII,[138] kindly provided by Victor Steimle (University of Sherbrooke, Canada), into the pCMV-Tag2B vector. Myc-NLRC5 constructs are described in.[37] FLAG-Sin3A was generated by molecular cloning from pMSCV ires/GFP hSin3A[139] into the pCMV-Tag2B vector. FLAG-NELFB was kindly provided by Patrick Mehlen (Research Cancer Center of Lyon). All plasmids (inserts, tags and flanking regions) were verified by Sanger Sequencing.

siRNA-mediated silencing

HeLa Flp-In GFP and GFP-NLRC5 cells were transfected with 20 nM (siNT, siSin3A) or 10 nM (siCOBRA1) siRNA using HiPerFect transfection reagent (Qiagen) according to the manufacturer's conditions. AllStars Negative Control siRNA (SI03650318, Qiagen), siSIN3A_5 (SI02781240, Qiagen), siSIN3A_6 (SI03047611, Qiagen) and siCOBRA1_7 (SI04347854, Qiagen) were used. Knockdown was performed for 48 h and efficiency monitored by qRT-PCR or immunoblot.

Co-immunoprecipitation

Co-immunoprecipitation of GFP-NLRC5 from HEK293T cells, transiently transfected with Lipofectamine 2000 (Thermo Fisher Scientific), or from HeLa Flp-In GFP and GFP-NLRC5 cell lines was performed with GFP-Trap Agarose resin (Chromotek). Co-immunoprecipitation of FLAG-tagged NLRC5 constructs, FLAG-tagged Sin3A or FLAG-tagged NELFB from HEK293T cells, transiently transfected with Lipofectamine 2000 (Thermo Fisher Scientific), was performed with anti-FLAG M2 affinity gel (Sigma-Aldrich). Cells were lysed in NP-40 buffer for GFP pulldown [10 mM Tris/HCl pH 7.5 150 mM NaCl, 0.5 mM EDTA, 0.5% NP-40, 100 nM β-glycerophosphat, 100 nM sodium orthovanadate, 1 mM NaF and cOmplete Mini Protease inhibitor Cocktail (Roche)] and in Triton buffer for pulldown of FLAG-tagged NLRC5 constructs [10 mM Tris/HCl pH 7.5, 150 mM NaCl, 0.5 mM EDTA, 1% Triton-X100, 100 nM β-glycerophosphat, 100 nM sodium orthovanadate, 1 mM NaF and cOmplete Mini Protease inhibitor Cocktail (Roche)]. For pulldown of FLAG-tagged Sin3A or FLAG-tagged NELFB, cells were lysed in modified NP-40-HEPES buffer [10 mM HEPES, 50 mM NaCl, 0.1 mM EDTA, 0.1 mM EGTA, 0.1% NP-40 100 nM β-glycerophosphate, 100 nM sodium orthovanadate, 1 mM NaF and cOmplete Mini Protease Inhibitor Cocktail (Roche)]. Lysates were cleared by centrifugation (10 min, 4°C, 20,000 x g for GFP pulldown and 10 min, 4°C, 2,000 x g for FLAG pulldown) before the supernatants were loaded onto the matrix. Precipitation was performed at 4°C for 3 h before matrix was washed with lysis buffer. Proteins were identified by immunoblot.

Immunoblotting

Proteins were separated by Laemmli SDS-PAGE and transferred to a nitrocellulose membrane (Amersham™ Protran®). Proteins were detected by incubation of the membrane consecutively with primary and secondary antibodies and finally with Clarity Western ECL Substrate (BioRad) or SuperSignal West Femto Maximum Sensitivity Substrate (Thermo Fisher Scientific). Signals were recorded on an electronic camera system (Vilbert Fusion FX). Primary antibodies used: anti-GFP (Roche 11 814 460 001), anti-PPARγ (Cell Signaling #2443), anti-FLAG (Sigma-Aldrich F3165), anti-myc (Sigma-Aldrich M4439), anti-HLA-B (Santa Cruz sc-55582), anti-HLA-B/C (kind gift from Victor Steimle, University of Sherbrooke, Canada), anti-GAPDH (Santa Cruz sc-25778). Secondary antibodies used: goat anti-mouse IgG HRP conjugate (BioRad #170-6516), goat anti-rabbit IgG HRP conjugate (BioRad #170-6515) and goat anti-mouse light chain specific-HRP conjugate (Jackson ImmunoResearch #115-035-174).

qRT-PCR

qRT-PCR was performed using iQ SYBR Green Supermix (BioRad) or GreenMasterMix (Genaxxon) according to the manufacturer's instructions on cDNA obtained from isolated RNA of the indicated cell lines or animal tissues. For cell lines, RNA was isolated using the RNeasy Plus Mini kit (Qiagen). For animal tissue, 100 mg adipose tissue or 30 mg liver were homogenized in 900 µL Qiazol in Lysing Matrix D 2 mL tubes (MP Biomedicals) using the FastPrep®-24 Tissue and Cell Homogenizer (MP Biomedical) at 6.0 m/s for 40 sec. Homogenates were centrifuged for 10 min at 12,000 x g at 4°C and RNA was isolated from the resulting supernatants using the RNeasy Plus Universal kit (Qiagen) according to manufacturer's instructions. 400 ng or 800 ng of total RNA was transcribed into cDNA using iScript cDNA Synthesis kit (BioRad) according to the manufacturer's instructions. Data is shown as normalized mean expression of each biological replicate determined in technical duplicates. The following primer pairs were used:

Target, Ref.	Primer fwd	Primer rev
CD36[78]	AGATGCAGCCTCATTTCCAC	GCCTTGGATGGAAGAACAAA
FABP4[78]	AACCTTAGATGGGGGTGTCC	GTGGAAGTGACGCCTTTCAT
GAPDH	GGTATCGTGGAAGGACTCATGAC	ATGCCAGTGAGCTTCCCGTTCAG
H2K[106]	TTGAATGGGGAGGAGCTGAT	GCCATGTTGGAGACAGTGGA
HLA-A[39]	AAAAGGAGGGAGTTACACTCAGG	GCTGTGAGGGACACATCAGAG
Hprt[140]	CCCTGGTTAAGCAGTACAGCCCC	AGTCTGGCCTGTATCCAACACTTCG
NELFB	GGAGCCCAAGATGGAGGT	CTCCTGCAGAAACTTAGTGAAG
Nlrc5	TTGATGGGTTGGATGAGGCT	CAAAGCCCCACATGTGTACC
NLRC5	CTCCTCACCTCCAGCTTCAC	GTTATTCCAGAGGCGGATGA
Sin3A[141]	CAGAATGACACCAAGGTCCTGAG	CATACGCAAGTGAGAGGTGTGG
Tgf-b	AGGAGACGGAATACAGGGCT	GGATCCACTTCCAACCCAGG
Tnf-a	AGAACTCCAGGCGGTGC	AGGGTCTGGGCCATAGAACT

Indirect immunofluorescence

HeLa Flp-In cells were seeded on glass coverslips and expression of the indicated GFP-NLRC5 constructs was induced by 1 μg/mL doxycycline overnight. Cells were fixed with 4% PFA in PBS, permeabilized with 0.5% Triton X-100 and blocked with 5% FBS in PBS. DNA was stained with Hoechst 33258 (Sigma). Images were captured with a Leica DMi8 microscope using a HCX PL FL L 40X/0.60 objective and processed using the Leica LasX software.

Measurement of cytokines

TNF-α release was measured in cell supernatants by ELISA (DY410, R&D Systems) according to the manufacturer's instructions.

Luciferase reporter gene assays

Briefly, 3 × 10^4 HEK293T cells/well were seeded in 96-well plates. Cells were transfected with 10 ng of a β-galactosidase-encoding plasmid, 20 ng of the HLA-B250 luciferase reporter plasmid, 0.5 ng of GFP-NLRC5 and the indicated amounts of FLAG-Sin3A using XtremeGene 9 (Sigma-Aldrich) according to the manufacturer's instructions. 16–24 h post transfection, cells were lysed in 100 μL lysis buffer and the luciferase activity was measured in a multiplate reader (Enspire, PerkinElmer LifeSciences) after addition of 100 μL reading buffer. Luciferase activity was normalized to β-galactosidase activity. See also.[37]

Yeast two-hybrid screening

An ULTImate yeast two-hybrid (Y2H) screen was performed by Hybrigenics, Paris. The N-terminal domain of human NLRC5 (amino acids 1–139) was used as bait and cloned into pB66 and pB35 vectors to encode for GAL4-NLRC5 DD fusion proteins, which encompass the DNA binding domain of the Regulatory protein Gal4 of *Saccharomyces cerevisiae*. Screening was performed with both constitutive pB66 and inducible pB35 vectors at 0.5 mM 3AT against a human thymocyte cDNA prey library prepared form $CD4^+$ and $CD8^+$T cells. Results were scored by global predicted biological score (PBS®) ranking.[142]

QUANTIFICATION AND STATISTICAL ANALYSIS

Data were analysed by two-way ANOVA with Tukey's multiple comparisons test, unpaired t-test or Kruskal-Wallis test. (Adjusted) p-value ≤ 0.0332 was regarded as significant. Data was analysed and plotted using GraphPad Prism version 7.00.